ABSTRACT

ACCURACY OF SEMI-INFINITE DIFFUSION THEORY TO ESTIMATE TISSUE HEMODYNAMICS IN LAYERED SLAB MODELS

by Md. Mainul Hasan Sabbir

Diffuse optical spectroscopy (DOS) is a widely used non-invasive technique to study the morphology and function of biological tissues. DOS measurements are usually acquired using fiber-based measurements of diffuse reflectance which are then analyzed using theoretical models of photon propagation to compute the absorption and scattering coefficients. These optical properties in turn can be related to important physiological parameters, such as hemoglobin concentration or oxygen saturation. Diffusion theory (DT) is widely utilized for quantifying DOS reflectance measurements from biological tissues given its compact analytic nature, but DT represents the tissue media using homogeneous optical properties. Many biological tissues, such as brain, have layered structure with inhomogeneous optical properties. Monte Carlo (MC) methods are also widely utilized rigorous solvers for photon transport in turbid media which can easily be used to incorporate spatial heterogeneity in the medium. In this study, two-layered slab tissue models will be utilized to simulate diffuse reflectance at multiple wavelengths. By analyzing reflectance spectra using DT, the accuracy of the diffusion theory to estimate physiological parameters will be studied.

ACCURACY OF SEMI-INFINITE DIFFUSION THEORY TO ESTIMATE TISSUE HEMODYNAMICS IN LAYERED SLAB MODELS

Thesis

Submitted to the

Faculty of Miami University

in partial fulfillment of

the requirements for the degree of

Master of Physics

by

Md. Mainul Hasan Sabbir

Miami University

Oxford, Ohio

2021

Adviser: Dr. Karthik Vishwanath

Reader: Dr. Paul Urayama

Reader: Dr. Imran Mirza

©2021 Md. Mainul Hasan Sabbir

This thesis titled

ACCURACY OF SEMI-INFINITE DIFFUSION THEORY TO ESTIMATE TISSUE HEMODYNAMICS IN LAYERED SLAB MODELS

by

Md. Mainul Hasan Sabbir

has been approved for publication by

College of Arts and Science

and

Department of Physics

Dr. Karthik Vishwanath

Dr. Paul Urayama

Dr. Imran Mirza

Contents

1 Introduction **1**

1.1 Background and Motivation 1

1.2 Thesis Organization 3

1.3 Definitions 4

1.4 Measurement Techniques 5

1.5 Objectives 6

2 Theoretical Methods and Preliminary Analysis **7**

2.1 Radiative Transport Equation 7

2.1.1 Diffusion Theory 8

2.2 Monte Carlo Method 10

2.3 Comparison of Diffusion Theory with MC: Semi-infinite Models 11

2.3.1 Forward Model 11

2.3.2 Inverse Model 13

3 Tissue Models **17**

3.1 Calculating Optical Coefficients 17

3.2 Semi-infinite Models 19

3.3 Layered Slab Models 20

4 Analysis and Results **23**

4.1 Derived Physiological Parameters 23

4.2 Analysis: Semi-infinite Tissue Models 24
4.3 Analysis: Layered Slab Tissue Models 28

5 Conclusion **32**
5.1 Summary of the Findings 32
5.2 Future Directions 33

Bibliography **41**

List of Tables

1.1 *Summary of the units of the described quantities used in this study.* 4

2.1 *The representation of each term in radiative transport equation.* 8

2.2 *Absorption and scattering coefficients of four tissue models used for the purpose of preliminary analysis.* 11

3.1 *Derived parameters "a and b "for brain and muscle tissue and the absorption coefficients for three wavelengths.* 19

3.2 *Calculation of the number of semi-infinite tissue models used for this study.* 20

3.3 The derived parameters a and b used for the superficial layer of brain and muscle tissue and the values of μ_s' at mentioned wavelengths. 21

3.4 *Calculation of the number of layered slab tissue models used for this study.[B stands for bottom and S stands for superficial layer.]* 22

List of Figures

1.1 *(a) Portable pulse oximeter to monitor tissue oxygenation [5]. (b) Measurement of brain activity using diffuse optical spectroscopy [3]. (c) Schematic diagram of diffuse optical spectroscopy.* 1

1.2 *Measurement techniques utilized in this study. Here, I_0 is the intensity of the incident light, and I_1 and I_2 are the intensity of the diffused light. ρ is the source-detector separation.* 5

2.1 *The figure shows the geometry for the calculation of diffuse reflectance from a pencil-source beam incident upon a semi-infinite turbid medium [22].* 8

2.2 *The figure shows the comparison of time-domain diffuse reflectance calculated using diffusion theory (black lines) with Monte Carlo simulations (colored lines) at ρ = 0.35, 0.75 1.25 and 1.75 cm for all the tissue models in the table 2.2.* 12

2.3 *The figure shows the comparison of steady state diffuse reflectance for all the tissue models (table 2.2) calculated using diffusion theory (black lines) with Monte Carlo simulations (colored lines).* 13

2.4 *The figure shows the basic workflow of the diffusion theory as an inverse model.* . . 14

2.5 *The figure shows the fitted data from the inverse model using diffusion theory (black lines) along with the Monte Carlo simulations (colored lines) at ρ = 0.35, 0.75 1.25 and 1.75 cm for all the tissue models (table 2.2). In the legend, the bracket indicates the percentage of error in retrieved optical coefficients.* 15

2.6 *(a) The figure shows the average percentage error in recovered (a) absorption and (b) reduced scattering coefficient of all the tissue models in the table 2.2 at source-detector separation ranging from 0.35 to 2.45 cm.* 15

2.7 *(a) The figure shows the average percentage error in recovered absorption and reduced scattering coefficients from the steady state measurements depending on the range of source-detector separation considered for the fitting purpose. (b) The figure shows the fitted steady state reflectance data from the inverse model using diffusion theory (black lines) along with the Monte Carlo simulations (colored lines).* 16

3.1 *The figure shows how to calculate absorption and reduced scattering coefficient using relevant quantities.* 18

3.2 *Schematic diagram of layered slab tissue model for brain and muscle.* 20

4.1 *The figure shows the average percentage of error of the recovered absorption, μ_a and reduced scattering coefficient, μ'_s in time domain at source-detector separation from 0.75-1.75 cm. The recovered reduced scattering coefficients bars are scaled down by a factor 15 for the plotting purposes (the error bars are not scaled).* 25

4.2 *The figure shows percentage of error of the recovered absorption, μ_a and reduced scattering coefficient, μ'_s in steady state for all the 27 tissue models of brain and muscle.* 25

4.3 *The figure shows the recovered HbT and StO_2 in steady state. The blue points represents muscle tissue and the black points for brain tissue. The circle, cross and square points represent three different StO_2 that are considered(irrespective of color). The points are scattered into three groups as three HbT are considered for each tissue type. The red line is the fitted line and the slope of the fitted lines are mentioned in the bracket of the legend. The black line represents the exact line where true values are equal to the retrieved values from the inverse model (or, $y = x$; slope = 1). In the legend, the slope of fitted line is shown inside the bracket.* . . 26

4.4 *The figure shows the recovered HbT and StO_2 in time domain. The points and lines properties are kept the same as in the figure 4.3. Each row represents the data at each source-detector separation (ρ = 0.75, 1.25 and 1.75 cm). The first column of figures are for recovered HbT and second column of figures are for recovered StO_2.* 27

4.5 *In the figure, the first column is for layered slab model and the second column for the semi-infinite model. The first row shows the fitted data with the MC simulated diffuse reflectance in time domain from a layered slab and a semi-infinite model. The optical coefficients for the layered slab model are: S: $\mu_a = 0.08\ cm^{-1}$, $\mu'_s = 13.69\ cm^{-1}$; B: $\mu_a = 0.13\ cm^{-1}$, $\mu'_s = 15.78\ cm^{-1}$. [S - superficial layer, B - bottom layer.] The semi-infinite model has the same optical properties as the bottom layer of the layered slab model. In the legend of the first row, the squared norm of the residuals are mentioned. The second row shows the change of the residuals with time.* 28

4.6 *The average percentage of error of recovered optical coefficients with respect to the thickness of the superficial layer at $\rho = 0.75$, 1.25 and 1.75 cm in time domain.* 29

4.7 *The average percentage of error in recovered HbT and StO_2 for different thicknesses of the superficial layer at ρ = 0.75 (row 1), 1.25 (row 2) and 1.75cm (row 3). The first column are for HbT and the second column is for StO_2. The factors shown in the legend are used to make the bar visible.* 31

Dedication

"To my mother and Ms. Martha Petrone for their unwavering support and belief in me"

Acknowledgements

I would first like to thank my advisor, Dr. Karthik Vishwanath, for the guidance throughout the project. I also like to thank Dr. Paul Urayama and Dr. Imran Mirza for taking the time to read and critically analyze my writing. I will always be grateful for the kind support I received from Dr. Mahmud Khan during the course of this study that helped me to focus solely on my research. Moreover, I would like to thank my friend S.M. Mustaquim for tolerating me during this stressful journey. Lastly, my time in Oxford would have been so different without Ms. Martha Petrone. Your moral support and kindness made it easy for me to navigate during the most difficult times of my life.

Chapter 1

Introduction

1.1 Background and Motivation

Next time you go to a clinic, you will observe that your doctor probably use pulse oximeter to measure oxygen saturation level (figure 1.1a) or hemoglobinometer to measure hemoglobin concentration. Physiological parameters such as, total hemoglobin concentration (HbT), oxygen saturation (StO_2) are crucial in many diagnostic and therapeutic applications[1–4]. The technique involved behind these instruments is called Diffuse optical spectroscopy (DOS). DOS is a widely

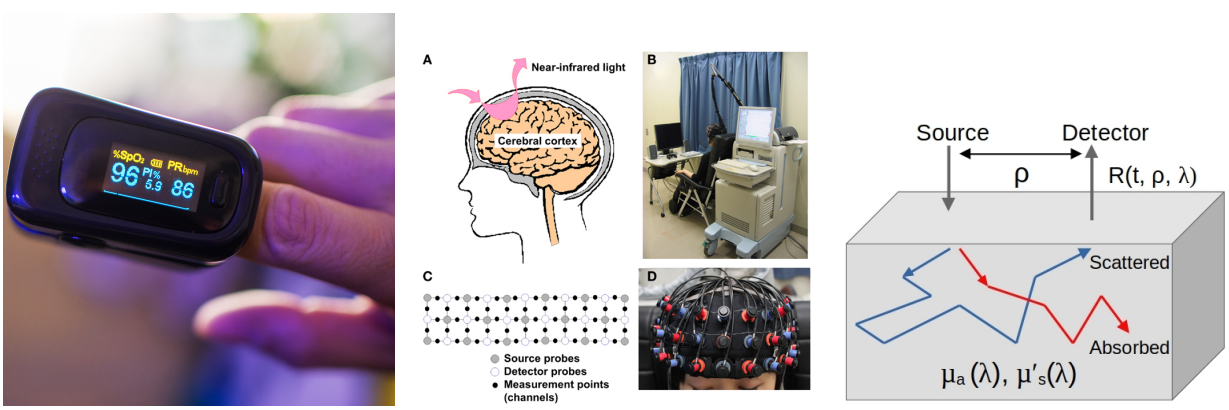

(a) (b) (c)

Figure 1.1: *(a) Portable pulse oximeter to monitor tissue oxygenation [5]. (b) Measurement of brain activity using diffuse optical spectroscopy [3]. (c) Schematic diagram of diffuse optical spectroscopy.*

used noninvasive technique that utilizes light-tissue interaction [6–9]. Biological tissues interact with light in the form of absorption or scattering of photons. The unabsorbed fraction of the incident photons emerges from the tissue surface as diffuse reflectance, R(t, ρ, λ).

Light-tissue interaction is governed by wavelength-dependent quantities, that is, scattering and absorption coefficient (definitions are in section 1.3) [10, 11]. Theoretical models are required to estimate optical coefficients from the diffuse reflectance obtained from DOS measurements [12]. Using these coefficients, physiological parameters (i.e., HbT, StO_2) can be derived [13]. The radiative transport equation (RTE) analytically describes photon propagation in biological tissue [10, 11]. However, it has been analytically solved only for a few simple cases and it is computationally intensive to solve it numerically. Due to the long simulation time needed with numerical methods, the RTE is often approximated by the diffusion theory [14].

Diffusion theory (DT) is a widely employed model to obtain optical properties of biological tissues by analyzing diffuse reflectance spectra [10, 11]. The advantage of using the DT is that its solution can be obtained in analytical form for relevant geometries and it is computationally efficient [15–17]. If the optical properties of a homogeneous medium (optical properties are the same within the medium) are known, DT can model the diffuse reflectance spectra, hence operating as a forward model. Conversely, if the diffuse reflectance spectra of a media is known, DT can operate as an inverse model that can extract optical properties by iteratively running forward models to match measured diffuse reflectance with the calculated diffuse reflectance from DT [12].

An alternative approach to solve the RTE can be obtained numerically that can provide diffuse reflectance spectra given the optical properties of a medium. This approach is known as the Monte Carlo (MC) method that solves the RTE by random sampling with any desired accuracy if the required computational load is affordable [18]. It is regarded as the gold standard method to model photon transport in biological tissues. For this reason, the MC method is widely utilized as a reference to validate other less rigorous methods such as DT [16, 17, 19]. Another advantage of

the MC method is that it can simulate photon transport both in homogeneous and nonhomogeneous tissue models [18]. However, inverse MC method is computationally intensive for multi-wavelength analyses to obtain optical properties, therefore, the derived clinical parameters (HbT, StO_2), though it is accurate [20].

In practice, measurements of diffuse reflectance are analyzed utilizing DT to obtain optical properties, though it assumes biological tissue as a homogeneous one-layered medium with a semi-infinite geometry (by convention, the length dimension of the tissue along the Z axis is considered infinite) [10, 11]. However, many tissues have layered tissue structure. For example, a brain tissue has layers of scalp and skull and a muscle tissue has layers of skin and subcutaneous fat. The optical properties varies over the layers because of the presence of chromophores. Chromophores, mainly hemoglobin and melalin, are responsible for the absorption of light, hence have an impact on the diffuse reflectance spectra [21]. Therefore, the question is that how well diffusion theory works if layered tissue models are used instead of semi-infinite tissue models and how much impact layered tissue structure has on the derived clinical parameters.

The main goal of this thesis is to analyze diffuse reflectance spectra of layered slab tissue models using DT to determine the extent of error in total hemoglobin concentration (HbT) and oxygen saturation (StO_2). So, by utilizing in-house developed layered MC model, diffuse reflectance spectra at multiple wavelengths for several HbT and StO_2 values will be simulated for both semi-infinite and two-layered tissue models. Then by developing an inverse model using DT, the optical properties of all the tissue models will be recovered. Then the extracted absorption coefficients will be used to examine the errors between recovered and input HbT and StO_2 values.

1.2 Thesis Organization

In this chapter, a short introduction on the relevant definitions, measurement techniques used in this study as well as the objectives are provided. Chapter 2 describes theoretical and computational models and it is followed by preliminary validations. In chapter 3, the development of semi-infinite

and layered slab models are discussed. Chapter 4 describes the procedure to derive physiological parameters from recovered optical properties as well as the analyses and results. Finally, chapter 5 concludes this thesis with a summary of the findings and possible avenues of future investigation.

1.3 Definitions

This section defines relevant optical parameters and optical properties that are used to describe the photon propagation in a tissue. The unit of measurement of all the parameters are shown in the table 1.1.

Absorption ($\mu_a(\lambda)$) and Scattering ($\mu_s(\lambda)$) Coefficient: The absorption and scattering coefficient express the inverse mean free path traveled by a photon between successive absorption or scattering events within the medium respectively.

Anisotropy factor, g: It defines the mean cosine of scattering angle by photon from an incoming direction. It is a dimensionless quantity.

$$g = \langle \cos\theta \rangle \tag{1.1}$$

Reduced Scattering Coefficient, $\mu_{s'}(\lambda)$: It is defined as $\mu_s' = \mu_s(1-g)$.

Quantity	Symbol	Unit
Absorption coefficient	μ_a	cm^{-1}
Scattering coefficient	μ_s	cm^{-1}
Reduced scattering coefficient	$\mu_{s'}$	cm^{-1}
Anisotropy factor	g	Dimensionless
Radiance	$L(\mathbf{r}, \hat{\mathbf{s}}, t)$	$Wcm^{-2}Sr^{-1}$
Fluence Rate	$\Phi(\mathbf{r}, t)$	Wcm^{-2}
Total Hemoglobin Concentration	HbT	μM
Oxygen Saturation	StO_2	Dimensionless

Table 1.1: *Summary of the units of the described quantities used in this study.*

Radiance, $L(\mathbf{r}, \hat{\mathbf{s}}, t)$: Radiance is the quantity used to describe the propagation of photon energy. It is defined as the average power that at position **r** and time t flows through the unit area oriented in the direction of the unit vector $\hat{s}$ moving within the unit solid angle around $\hat{s}$.

Fluence Rate, $\Phi(\mathbf{r}, t)$: Fluence rate is defined as the integral of the radiance over all directions.

$$\Phi(\mathbf{r}, t) = \int L(\mathbf{r}, \hat{\mathbf{s}}, t) \tag{1.2}$$

Total Hemoglobin Concentration, HbT: The total hemoglobin concentration is defined as the sum of the concentration of oxyhemoglobin(HbO_2) and deoxyhemoglobin (Hb).

$$[HbT] = [HbO_2] + [Hb] \tag{1.3}$$

Oxygen Saturation, StO_2: The oxygen saturation is the ratio of the concentration of oxyhemoglobin (HbO_2) and the total hemoglobin concentration (HbT).

$$StO_2 = \frac{[HbO_2]}{[HbO_2] + [Hb]} = \frac{[HbO_2]}{[HbT]} \tag{1.4}$$

1.4 Measurement Techniques

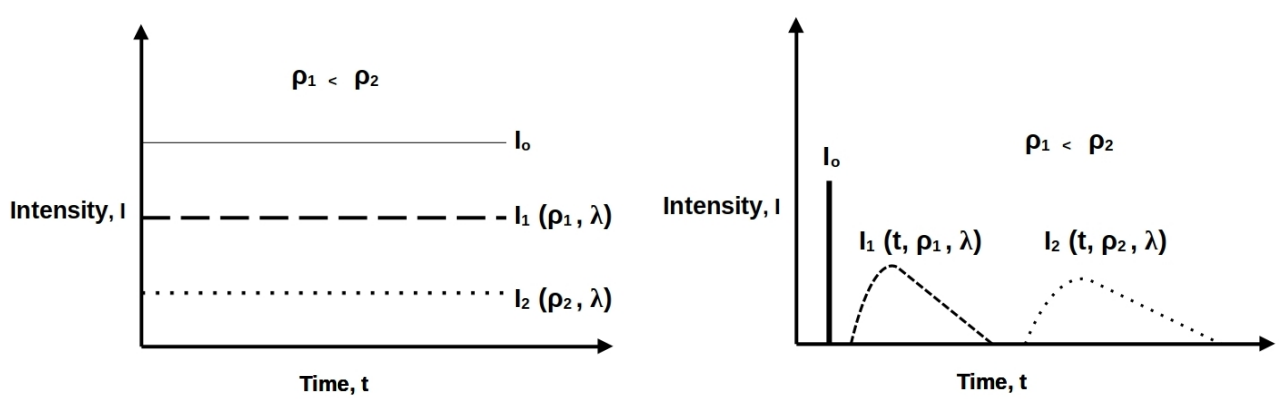

(a) *Steady state diffuse optical spectroscopy.* (b) *Time-domain diffuse optical spectroscopy.*

Figure 1.2: *Measurement techniques utilized in this study. Here, I_0 is the intensity of the incident light, and I_1 and I_2 are the intensity of the diffused light. ρ is the source-detector separation.*

DOS measurement techniques can be categorized into three methods to obtain diffuse reflectance spectra. They are known as steady-state, time-domain and frequency-domain. In this study,

steady state and time-domain technique will be explored. In steady state technique, it requires a monochromatic source emitting light at a constant intensity and a series of detectors (several source-detector separation) to extract optical properties from the diffuse reflectance spectra. This is also known as spatially-resolved steady state technique. In steady state technique, the intensity of the incident light decreases with the source-detector separation, ρ (figure 1.2a). In the time-domain, short pulses of light (usually in picosecond order) is used to illuminate the tissue to obtain the temporal distribution of photons at a certain source-detector separation. The distribution is known as temporal point spread function (TPSF). TPSF extend over several nanoseconds after propagating through the biological tissue and TPSF extend with increasing source-detector separation, ρ (figure 1.2b). The optical properties of the investigated tissue can be inferred from the shape of the TPSF [7].

1.5 Objectives

The primary goal of this thesis is to determine the extent of error in derived physiological parameters of layered slab tissue models using semi-infinite diffusion theory. The main tasks of this study can be summarized as:

1. Generating semi-infinite and layered slab tissue models from several pairs of hemoglobin concentration (HbT) and oxygen saturation (StO_2) for brain and muscle tissue to obtain optical coefficients.
2. Developing inverse model using semi-infinite diffusion theory both in steady state and time-domain to extract optical properties from the MC simulated measurements of diffuse reflectance.
3. Analyzing the accuracy of semi-infinite diffusion theory to calculate physiological parameters using retrieved optical properties from layered slab models.
4. Understanding the impact of the thickness of the superficial layer in derived physiological parameters from layered slab models.

Chapter 2

Theoretical Methods and Preliminary Analysis

2.1 Radiative Transport Equation

The radiative transport equation is derived from the principle of conservation of energy and it describes the energy transfer in the form of electromagnetic radiation [10, 11]. The time-resolved radiative transport equation has the following form:

$$\frac{1}{c}\frac{\partial}{\partial t}L(\mathbf{r},\hat{\mathbf{s}},t)+\hat{s}.\nabla L(\mathbf{r},\hat{\mathbf{s}},t)+[\mu_a(\mathbf{r})+\mu_s(\mathbf{r})]L(\mathbf{r},\hat{\mathbf{s}},t)=\mu_s(\mathbf{r})\int_{4\pi}p(\mathbf{s},\hat{\mathbf{s}}')L(\mathbf{r},\hat{\mathbf{s}}',t)d\Omega'+S(\mathbf{r},\hat{\mathbf{s}},t) \tag{2.1}$$

Here, c is the velocity of light within the medium, $q(\mathbf{r},\hat{\mathbf{s}},t)$ is the source term that is the power emitted at time t per unit volume and unit solid angle along $\hat{s}$, and $d\Omega$ is the solid angle in the direction $\hat{s}'$. The scattering phase function, $p(\mathbf{s},\hat{\mathbf{s}}')$ describes the probability of scattering from direction $\hat{s}'$ into direction $\hat{s}$ and $\mu_a(\mathbf{r})$ and $\mu_s(\mathbf{r})$ are the absorption and scattering coefficients respectively. The exact form of phase function, is usually complex, though it is generally taken as the Henyey-Greenstein phase function. The terms in equation (2.1) can be represented as follows (table 2.1) considering the volume element dV identified by the position vector, $\mathbf{r}$:

Term	Represents
$\frac{1}{c}\frac{\partial}{\partial t}L(\mathbf{r},\hat{\mathbf{s}},t)dVd\Omega dt$	The total temporal change of energy that is propagating along $\hat{s}$ within dV, $d\Omega$ and dt.
$\hat{s}.\nabla I(\mathbf{r},\hat{\mathbf{s}},t)dVd\Omega dt$	The net flux of energy that is propagating along $\hat{s}$ through the volume dV, within $d\Omega$, and dt.
$[\mu_a(\mathbf{r})+\mu_s(\mathbf{r})]I(\mathbf{r},\hat{\mathbf{s}},t)dVd\Omega dt$	The fraction of energy that is propagating along $\hat{s}$ within dV, $d\Omega$, and dt extracted by scattering and absorption phenomena
$\mu_s(\mathbf{r})\int_{4\pi}p(\mathbf{s},\hat{\mathbf{s}}')I(\mathbf{r},\hat{\mathbf{s}}',t)d\Omega' dVd\Omega dt$	The energy coming from any direction $\hat{s}'$ that, within, dV, $d\Omega$, and dt, is scattered in direction $\hat{s}$.
$q(\mathbf{r},\hat{\mathbf{s}},t)dVd\Omega dt$	The energy generated along $\hat{s}$ in $d\Omega$ and dt by sources inside dV.

Table 2.1: *The representation of each term in radiative transport equation.*

2.1.1 Diffusion Theory

Diffusion theory is a widely utilized model to describe photon propagation in biological tissue which is an approximation of radiative transport equation [10, 11]. The time-resolved diffusion equation for light transport in homogeneous tissue media can be written as following:

$$\frac{\partial\Phi(\mathbf{r},t)}{\partial t} = c[D\nabla^2\Phi(\mathbf{r},t) - \mu_a\Phi(\mathbf{r},t) + S(\mathbf{r},t)] \tag{2.2}$$

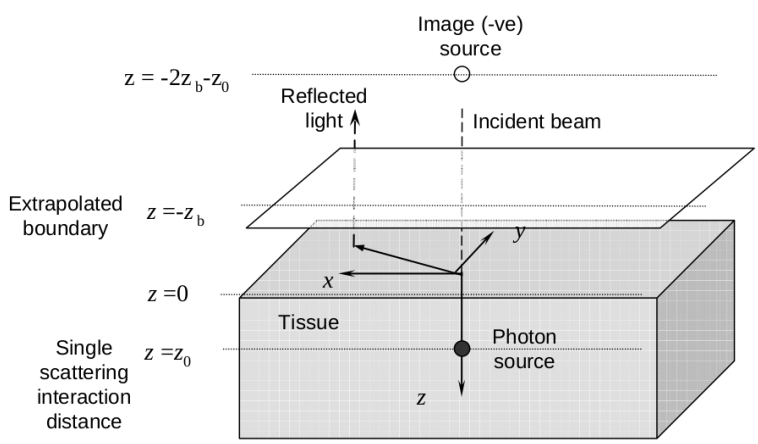

Figure 2.1: *The figure shows the geometry for the calculation of diffuse reflectance from a pencil-source beam incident upon a semi-infinite turbid medium [22].*

Here, $D = \frac{1}{3(\mu_a+\mu_s')}$ is known as the diffusion coefficient. The steady-state diffusion equation can be obtained from equation after setting the time derivative of fluence rate, $\Phi(\mathbf{r}, t)$ equal to zero.

The solution of diffusion equation for a semi-infinite turbid medium can be obtained applying extrapolated boundary condition. The extrapolated boundary condition implies that the fluence rate goes to zero some distance beyond the actual surface [17]. The solution of diffusion equation for the fluence rate, ϕ in time domain can be written as:

$$\Phi(\rho, z, t) = \frac{ce^{\mu_a ct}}{(4\pi Dct)^{3/2}}(e^{-\frac{(z-z_0)^2+\rho^2}{4Dct}} - e^{-\frac{(z+z_0+2z_b)^2+\rho^2}{4Dct}}) \tag{2.3}$$

Here, ρ is the radial distance from the source, and z is the distance normal to the boundary. The first term states a point source at $z_0 = (\mu_a + \mu_{s'})^{-1}$, and the second term implies a negative image source. For the zero-boundary condition, z_b is zero, whereas $z_b = 2D\frac{1+R_{eff}}{1-R_{eff}}$ for the extrapolated boundary condition. Here, R_{eff} represents the internally diffused reflected fraction of photons at the boundary. In the steady state, the fluence rate can be expressed as:

$$\Phi(\rho, z) = \frac{1}{4\pi D}(\frac{e^{-\mu_{eff}[(z-z_0)^2+\rho^2]^{1/2}}}{[(z-z_0)^2+\rho^2]^{1/2}} - \frac{e^{-\mu_{eff}[(z+z_0+2z_b)^2+\rho^2]^{1/2}}}{[(z+z_0+2z_b)^2)+\rho^2]^{1/2}}) \tag{2.4}$$

Here, $\mu_{eff} = [3\mu_a(\mu_a + \mu_s')]^{1/2}$. Now, the diffuse reflectance can be calculated as the current across the boundary, with

$$R_d(\rho, t) = -D \bigtriangledown \phi(\rho, z, t).(-\mathbf{z})|_{z=0} \tag{2.5}$$

Inserting equation (2.3) into equation (2.5) yields:

$$R_d(\rho, t) = \frac{e^{-\mu_a ct}}{2(4\pi Dc)^{3/2}t^{5/2}} \times [z_0 e^{-\frac{{r_1}^2}{4Dct}} + (z_0 + 2z_b)e^{-\frac{{r_2}^2}{4Dct}}] \tag{2.6}$$

In the above expression, $r_1^2 = z_0^2 + \rho^2$ and $r_2^2 = (z_0 + 2z_b)^2 + \rho^2$. Similarly, by inserting equation (2.4) into equation (2.5), the steady state diffuse reflectance becomes:

$$R_d^s(\rho) = \frac{1}{4\pi}[z_0(\mu_{eff} + \frac{1}{r_1})\frac{e^{-\mu_{eff} r_1}}{r_1^2} + (z_0 + 2z_b)(\mu_{eff} + \frac{1}{r_2})\frac{e^{-\mu_{eff} r_2}}{r_2^2}] \tag{2.7}$$

The above expressions (equation (2.6) and (2.7)) will be extensively utilized in this study to perform the analyses.

2.2 Monte Carlo Method

Monte Carlo (MC) method is an extensively utilized computational tool for simulating photon transport in complex tissue structure and source-detector geometries, and that makes MC useful to examine multiple experimental designs via model predictions [18]. In addition, MC produces more accurate solutions than diffusion theory while simulating low scattering medium where diffusion theory becomes invalid [23]. In general, in the MC simulation a point source of photons enter the surface of the tissue medium with a defined initial position and direction. The movement of photons depend on the two major choices: the mean free path for the absorption and scattering events and the scattering angle. The detail discussion on the rules of the photon propagation in the MC simulation can be found in the literature [18, 24].

An in-house developed MC model is used to simulate the remitted radially resolved time-domain diffuse reflectance, $R(t, \rho, \lambda)$ detected on the surface of tissue models [25]. A predetermined source-detector geometry and tissue model layout are provided as input to calculate the diffuse reflectance at each source-detector separation, ρ. In addition, it is also required to specify the number of photons to be simulated and the temporal resolution for the simulation. In this study, 30 millions number of photons is simulated and the temporal resolution is 10ps (picosecond) for each simulation. The refractive indices of the media (assumed to be in contact) directly above and below the tissue medium (air is considered) is required as well as the the total number of layers of each tissue model and the thickness of each layer and their refractive index.

2.3 Comparison of Diffusion Theory with MC: Semi-infinite Models

The diffusion theory and MC method function as a forward model. It implies that given the physiological and structural properties of a tissue medium, they can model diffuse reflectance. However, in experimental perspective, the measurements from the diffuse optical spectroscopy provides the diffuse reflectance spectra where the optical properties of the medium is unknown. An inverse model is required to extract optical properties from the measured diffuse reflectance. The inverse model utilizes a forward model that runs iteratively to match the diffuse reflectance from the diffuse optical spectroscopy measurements. So, to construct an inverse model, at first forward model needs to be verified. In the following sections, the diffusion theory is compared with MC simulated diffuse reflectance (instead of experimental measurements) as a forward model. Then by developing an inverse model, the extent of error in recovered absorption and reduced scattering coefficient is shown for four distinct semi-infinite tissue models (table: 2.2).

Tissue Model(μ_a, μ'_s)	μ_a (cm^{-1})	$\mu'_s(cm^{-1})$
TM1(low, high)	0.04	15.78
TM2(low, low)	0.07	8.52
TM3(high, low)	0.21	8.52
TM4(high, high)	0.28	15.78

Table 2.2: *Absorption and scattering coefficients of four tissue models used for the purpose of preliminary analysis.*

2.3.1 Forward Model

To compare diffusion theory with the MC simulated diffuse reflectance as a forward model, four semi-infinite tissue models are chosen where absorption and reduced scattering coefficients vary from high to low (table 2.2). The time-domain diffuse reflectance is computed using eq.2.6 at source-detector separation, ρ = 0.35, 0.75, 1.25 and 1.75cm to compare with the MC simulated reflectance. From the figure 2.2, it can be concluded that the diffusion theory shows better agreement with the MC simulated diffuse reflectance at long compared to short source-detector separation.

Moreover, tissue models with high scattering coefficient and low absorption (i.e., tissue model 1) shows better agreement. The tissue model 3 and 4 have high absorption coefficients, though tissue

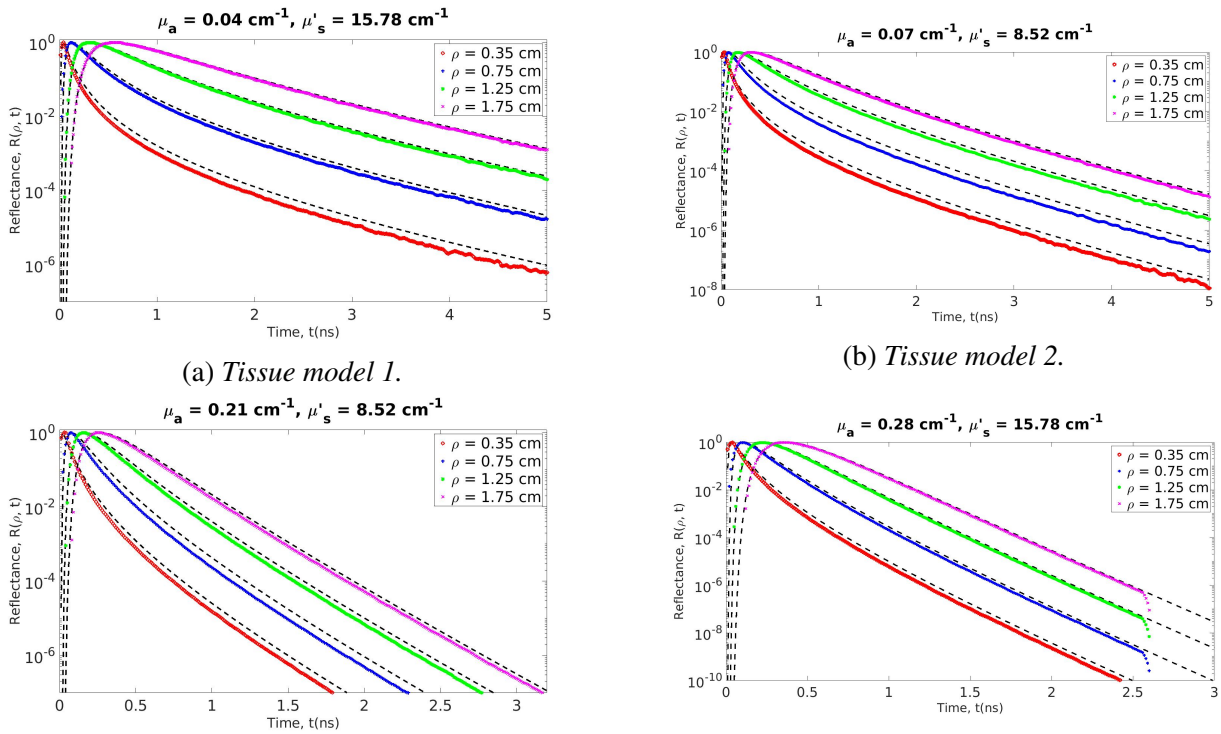

(a) *Tissue model 1.*

(b) *Tissue model 2.*

(c) *Tissue model 3.*

(d) *Tissue model 4.*

Figure 2.2: *The figure shows the comparison of time-domain diffuse reflectance calculated using diffusion theory (black lines) with Monte Carlo simulations (colored lines) at $\rho = 0.35$, 0.75 1.25 and 1.75 cm for all the tissue models in the table 2.2.*

model 4 shows better agreement as the reduced scattering coefficient is higher. In addition, the tissue models with the higher absorption coefficient, most of the photons get absorbed within the tissue media and that is the reason photons are not detected in the detector after 2-3 ns (i.e., tissue model 3 and 4). The steady state diffuse reflectance for all the tissue models are shown in the figure 2.3. By integrating time-domain diffuse reflectance over all the time range at each source-detector separation, the steady state diffuse reflectance is computed using the time-domain MC simulated diffuse reflectance. The steady state diffuse reflectance from the diffusion theory (computed using eq. 2.5) then compared.

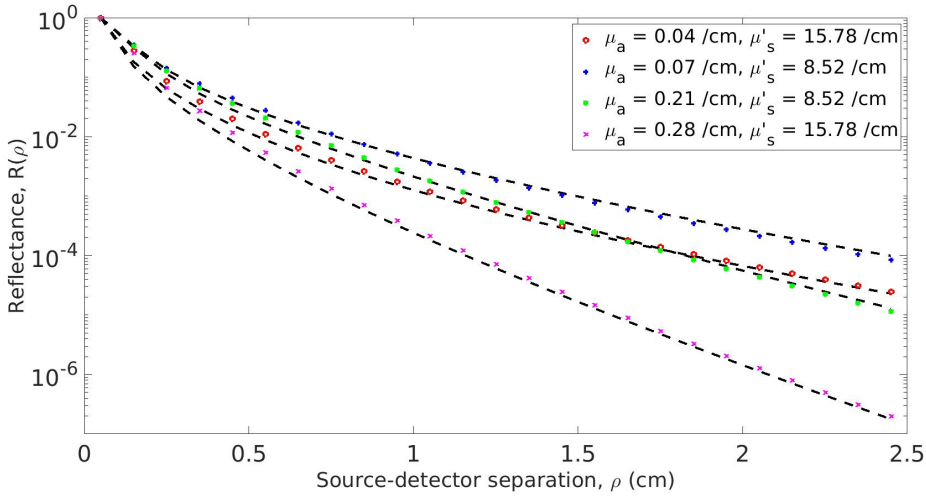

Figure 2.3: *The figure shows the comparison of steady state diffuse reflectance for all the tissue models (table 2.2) calculated using diffusion theory (black lines) with Monte Carlo simulations (colored lines).*

2.3.2 Inverse Model

In the previous section, the comparison between diffusion theory and the MC simulated reflectance is discussed as a forward model. To extract optical properties from the diffuse reflectance spectra, an inverse model is developed using the diffusion theory as a forward model. The figure 2.4 shows the flow chart of the inverse model that is used to fit diffuse reflectance spectra. First, an initial guess for the optical properties (μ_a, μ'_s) is made, and then the forward model (diffusion theory) is used to generate a spectrum. Next, the sum of squares error between the predicted reflectance and the measured reflectance is calculated. The free parameters, absorption and reduced scattering coefficient (μ_a, μ'_s), are then iteratively updated until the sum of squares error is minimized. For the fitting purposes, a nonlinear optimization routine (MATLAB function *lsqcurvefit*) is utilized to get the best fit of the theoretical model (diffusion theory) to the MC simulated diffuse reflectance.

The time-domain fitted data along with the MC data is shown in the figure 2.5 for all four tissue models (table 2.2). The time-domain MC data is fitted individually using eq.(2.6) with two free parameters μ_a and μ'_s. The temporal range for the fit is from the maximum peak at each source-detector separation, ρ for all the tissue models. The start time of the fitting gradually increased

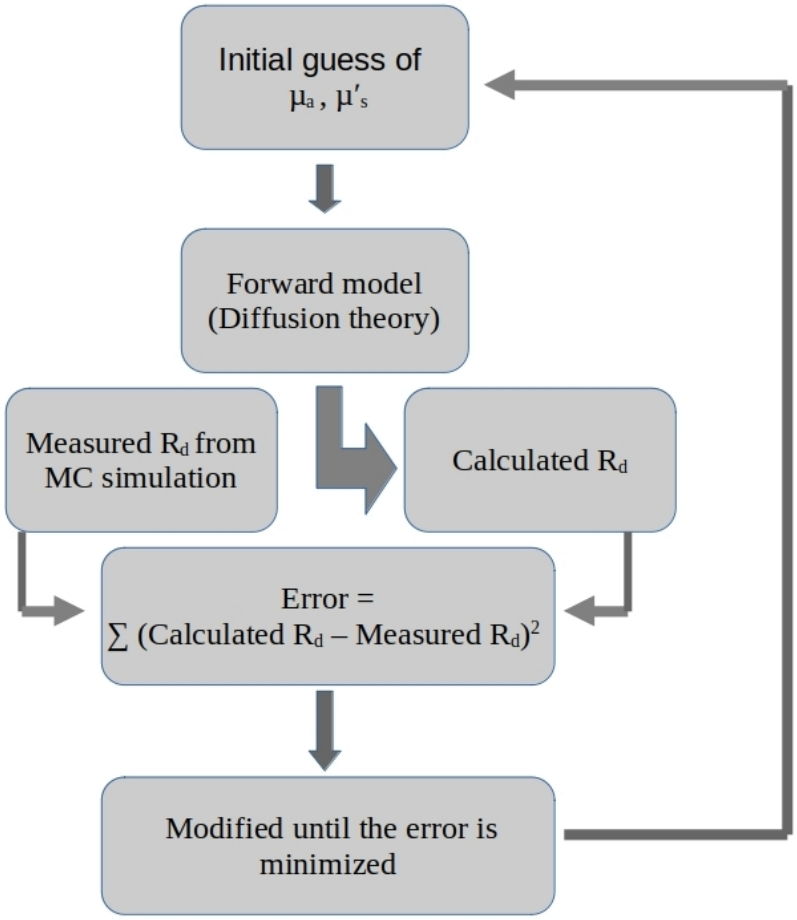

Figure 2.4: *The figure shows the basic workflow of the diffusion theory as an inverse model.*

due to the fact that the diffusion theory is least accurate at early times. So, the minimum start time of the fitting is around 0.1ns. The diffusion theory is valid if the photons experience many scattering interactions, i.e., $\mu'_s\rho >> 1$. For tissue models 1 and 4, $\mu'_s\rho$ varies 5.52 to 27.62 and for tissue models 2 and 3, it varies from 2.98 to 14.91. For each tissue models in the figure 2.5, it is observed that the greater the value of $\mu'_s\rho$, the percentage of error in recovered optical coefficient is reduced. Figure 2.5 also indicates that the error in recovered optical properties exceeds 40% if the $\mu'_s\rho < 6.5$ and it supports the findings of Kienle et al [17]. The average percentage of error of all the tissue models in table 2.2 are shown in figure 2.6 for source-detector separation, $\rho = 0.35 - 2.45cm$ and it depicts the fact that the percentage of error is higher for short source-detector separation.

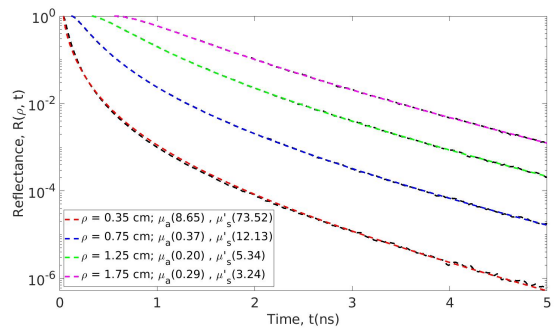

(a) *TM1:* $\mu_a = 0.04cm^{-1}, \mu_s' = 15.78cm^{-1}$

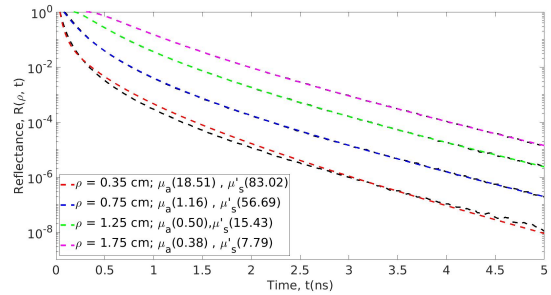

(b) *TM2:* $\mu_a = 0.07cm^{-1}, \mu_s' = 8.52cm^{-1}$

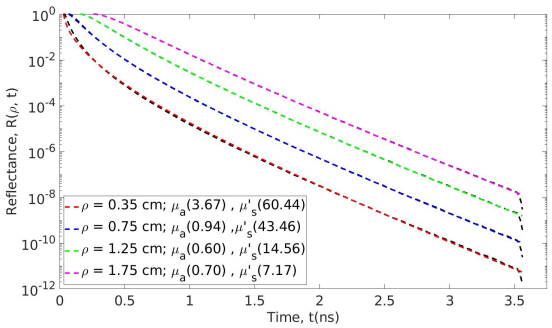

(c) *TM3:* $\mu_a = 0.21cm^{-1}, \mu_s' = 8.52cm^{-1}$

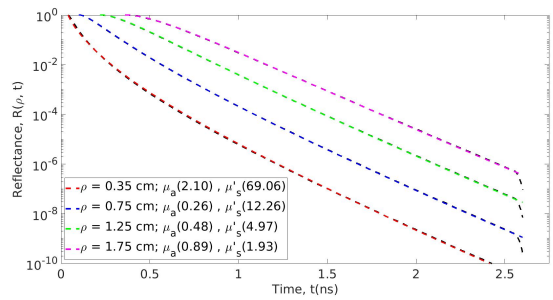

(d) *TM4:* $\mu_a = 0.28cm^{-1}, \mu_s' = 15.78cm^{-1}$

Figure 2.5: *The figure shows the fitted data from the inverse model using diffusion theory (black lines) along with the Monte Carlo simulations (colored lines) at $\rho = 0.35$, 0.75 1.25 and 1.75 cm for all the tissue models (table 2.2). In the legend, the bracket indicates the percentage of error in retrieved optical coefficients.*

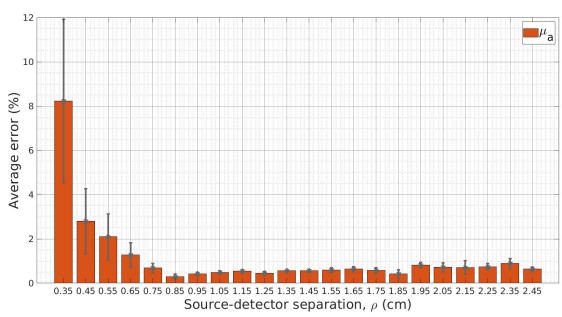

(a)

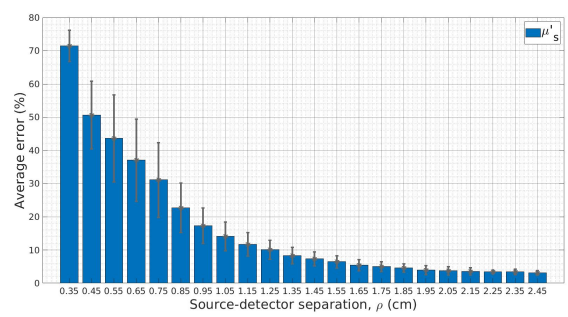

(b)

Figure 2.6: *(a) The figure shows the average percentage error in recovered (a) absorption and (b) reduced scattering coefficient of all the tissue models in the table 2.2 at source-detector separation ranging from 0.35 to 2.45 cm.*

To extract optical coefficients from the steady state spatially resolved diffuse reflectance, at first, it is analyzed how much impact the range of ρ has on the recovered optical coefficients. The figure

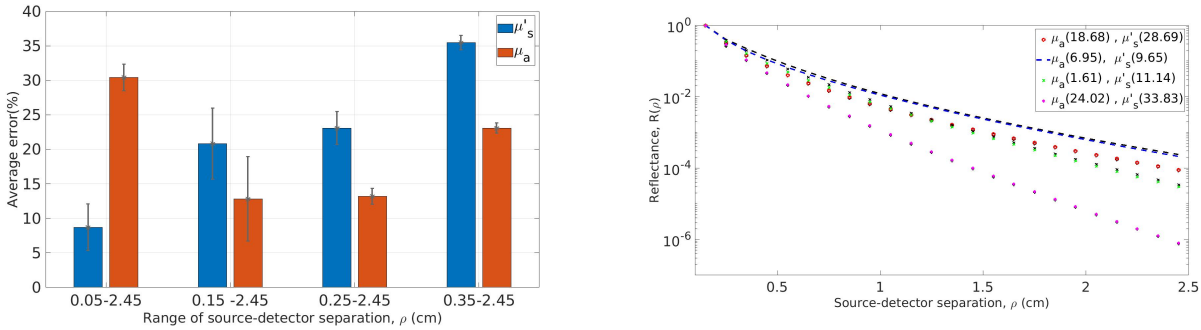

(a) (b)

Figure 2.7: *(a) The figure shows the average percentage error in recovered absorption and reduced scattering coefficients from the steady state measurements depending on the range of source-detector separation considered for the fitting purpose. (b) The figure shows the fitted steady state reflectance data from the inverse model using diffusion theory (black lines) along with the Monte Carlo simulations (colored lines).*

2.7a shows the average percentage of error for several range of source-detector separation. The error in recovered reduced scattering is quite low compared to the error in recovered absorption coefficient if all the ρ are considered while fitting. However, if we exclude the data for short source-detector separation, $\rho = 0.05$ cm, it is quite fascinating to observe that the percentage of error in recovered μ_s' becomes higher while the percentage of error in recovered μ_a becomes lower. Nonetheless, the observation from the time-domain analyses strengthen the fact that the diffusion theory is least accurate at short source-detector separation. For this reason, the steady state reflectance is fitted using weights calculated from $1/R_d$ while fitting to put more importance on the long source-detector separation steady state data. Moreover, the range of source-detector is chosen from $\rho = 0.15 - 2.45$ cm to fit steady state MC data as the percentage of error is comparable when $\rho = 0.05$ cm is excluded and when $\rho = 0.05, 0.15cm$ cm are excluded. The figure 2.7b shows the fitted data with MC simulated steady state diffuse reflectance.

Chapter 3

Tissue Models

In diffuse optical spectroscopy experiments with real tissue, the optical coefficients are extracted from the measurement of diffuse reflectance. Then using these optical coefficients physiological parameters, such as, HbT and StO_2, can be derived. In practice, this is the general procedure when diffusion theory is applied to obtain optical coefficients in order to compute physiological parameters of an unknown tissue model. In this thesis, to depict realistic tissue models, the derived physiological parameters will be used as inputs in simulation to generate the tissue models that are actually outputs from the experimental measurements of diffuse optical spectroscopy. In the following sections, the steps needed to generate semi-infinite and layered slab tissue models for brain and muscle from the physiological parameters are described. The tissue models will then be utilized to obtain MC simulated diffuse reflectance spectra.

3.1 Calculating Optical Coefficients

The absorption, μ_a and reduced scattering coefficient, μ_s' can be presented as a function of wavelength, λ. Though the equations are not exhaustive, they are sufficient to characterize the behavior of tissues like brain, muscle. skin etc [26]. The absorption coefficient, μ_a of a tissue can be expressed as the sum of contributions from all absorbing chromophores within the tissue:

$$\mu_a(\lambda) = ln(10)\Sigma_i(HbT)_i\varepsilon_i(\lambda) \tag{3.1}$$

Here, $\varepsilon(\lambda)$ is molar extinction coefficient of a chromophore and it measures how strongly a chromophore within the tissue medium attenuates light at a given wavelength. Any number of chromophores can be used to calculate $\mu_a(\lambda)$. In this study, hemoglobin is considered as the only source of chromophores (absorber). The values of molar extinction coefficient for hemoglobin at different wavelengths are tabulated by Prahl [27]. So, the eq.(3.1) can be rewritten in terms of oxygen saturation, StO_2 and the extinction coefficients for oxyhemoglobin, HbO_2 and deoxyhemoglobin, Hb at a wavelength, λ as:

$$\mu_a(\lambda) = ln(10)[(HbT).StO_2.\varepsilon_{HbO_2}(\lambda) + (HbT).(1 - StO_2).\varepsilon_{Hb}(\lambda)] \tag{3.2}$$

The total hemoglobin concentration, HbT and oxygen saturation, StO_2 varies depending on the tissue types and the values of HbT and StO_2 for different tissue types, such as brain, muscle and skin, are tabulated in the article by Jacques [26]. The figure (3.1a) shows the steps needed in order to compute absorption coefficient, μ_a at a certain wavelength, λ.

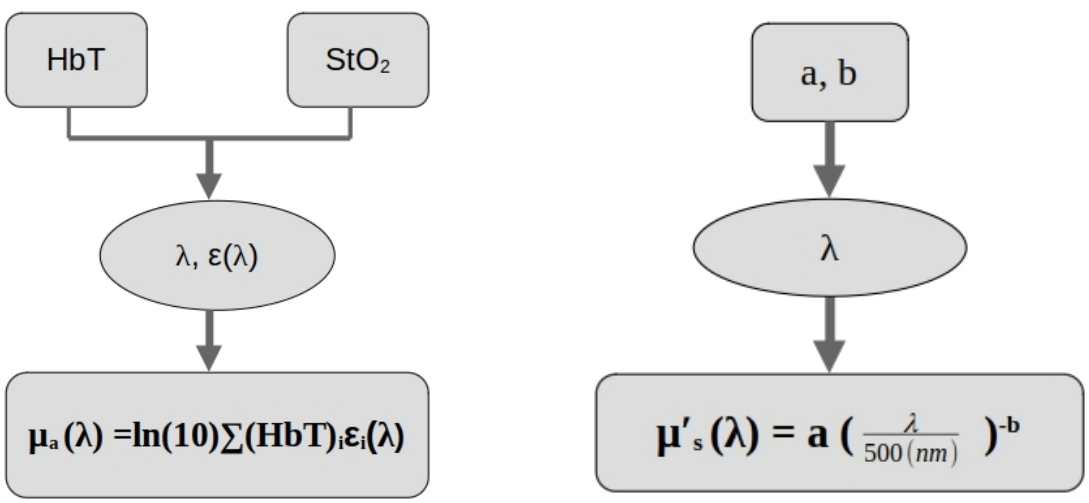

(a) (b)

Figure 3.1: *The figure shows how to calculate absorption and reduced scattering coefficient using relevant quantities.*

The reduced scattering coefficient, μ_s' at wavelength, $\lambda(nm)$ can be represented as:

$$\mu_s'(\lambda) = a(\frac{\lambda}{500(nm)})^{-b} \tag{3.3}$$

Here, in equation 3.3, the wavelength is normalized by a reference wavelength (500 nm) and this dimensionless quantity is raised to scattering power, b. This fractional term characterizes the wavelength dependence of reduced scattering coefficient, μ_s' and the factor "a(cm^{-1})"scales the fractional wavelength-dependent term The parameters "a, b "change depending on the tissue type. For example, skin and other fibrous tissue have higher values of "a"than other tissue types. The equation 3.3 is good for predicting tissue scattering within the wavelength range of 400-1300 nm. However, the equation diverge outside this wavelength range [26]. So, by specifying tissue parameters in equations 3.2 and 3.3, the optical properties of a generic tissue can be mimicked.

3.2 Semi-infinite Models

To construct semi-infinite tissue models (figure: **??**) for brain and muscle, four derived parameters (a, b, HbT, StO_2) are required. Then using equations 3.2 and 3.3, μ_a and μ_s' is calculated. The table 3.1 shows the values of derived parameters (a, b) considered for calculating reduced scattering coefficient, μ_s'. To compute absorption coefficient, μ_a, at first a base value of HbT and StO_2 are taken for brain and muscle. As the goal of this study is to determine the accuracy of semi-infinite diffusion theory to determine total hemoglobin concentration, HbT and oxygen saturation, StO_2, the base value of HbT and StO_2 of each tissue type is perturbed in order to get a range of absorption coefficient.

Tissue Type	a (cm^{-1})	b	Wavelength, λ (nm)	Reduced scattering coefficient, $\mu_s'(cm^{-1})$
Brain	40.8	3.089	680, 750, 830	15.78, 11.66, 8.52
Muscle	13	0.926	680, 750, 830	9.77, 8.93, 8.13

Table 3.1: *Derived parameters "a and b "for brain and muscle tissue and the absorption coefficients for three wavelengths.*

The base value of HbT is $65\mu M$ and $27\mu M$ for brain and muscle respectively [26]. The value

of HbT for each tissue type is then perturbed by 50% to get three different values of HbT (table 3.2). In addition, the base value for StO_2 is 0.7 for both brain and muscle tissue [26]. Then StO_2 is perturbed by 25% to get three unique values. The wavelengths chosen for calculating the optical coefficients are 680, 750 and 830 nm as they are standard wavelengths for diffuse optical spectroscopy measurements. So, for three unique values of HbT, StO_2 and λ, the total number of tissue models is 27 for each tissue type. In summary, the range of absorption coefficient, μ_a for brain ranges from 0.04 to 0.28 cm^{-1} and for muscle it ranges from 0.01 to 0.12 cm^{-1}.

Tissue type	HbT (μM)	StO_2	Wavelengths, λ (nm)	Number of models
Brain	32.5, 65, 97.5	0.53, 0.7, 0.88	680, 750, 830	27
Muscle	13.5, 27, 40.5	0.53, 0.7, 0.88	680, 750, 830	27

Table 3.2: *Calculation of the number of semi-infinite tissue models used for this study.*

3.3 Layered Slab Models

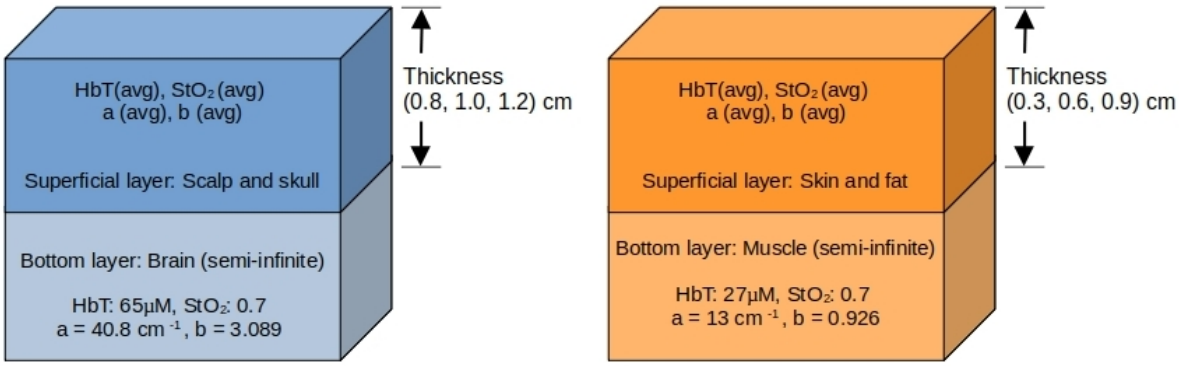

Figure 3.2: *Schematic diagram of layered slab tissue model for brain and muscle.*

The semi-infinite tissue models have homogeneous optical properties within the tissue media. However, in real tissue, the optical properties are heterogeneous. Moreover, real tissues have layered structure. For example, the brain has layers of scalp and skull. So, to mimic real tissue, the layered slab models can be utilized instead of semi-infinite tissue models. In this study, two-layered slab models are used where the brain and muscle tissue is accompanied by a superficial layer (figure

3.2). The superficial layer for brain consists of scalp and skull and for muscle it consists of subcutaneous fat and skin. In addition, the bottom layer (brain or muscle) is kept just like the semi-infinite tissue models and the thickness of the superficial layer will be varied to generate layered slab models.

To construct the bottom layer of layered slab models, the base value of derived parameters (HbT, StO_2, a and b) are kept the same as semi-infinite model's base value for brain and muscle as mentioned in the figure 3.2. So, for three different wavelengths (680, 750, 830 nm), three sets of optical coefficients (three unique bottom layer) can be computed for each tissue type. So, the reduced scattering coefficient, μ_s' for the bottom layer will be the same as mentioned in the table 3.2 for each tissue type. The absorption coefficient, μ_a for the brain ranges within 0.11 - 0.13 cm^{-1} and for the muscle it ranges within 0.04- 0.05 cm^{-1} for the mentioned three wavelengths.

For the superficial layer, the average base value of tissue components (i.e., scalp and skull for brain tissue) are considered. The table 3.3 shows the average derived parameters a_{avg} and b_{avg} considered for brain and muscle and the corresponding reduced scattering coefficient, μ_s' at three wavelengths. The base value of a and b of the components of superficial layer components can be found in these literatures [26, 28]. To compute the μ_a for the superficial layer of brain, the average of the derived parameters, HbT and StO_2 of scalp and skull, is computed. Then by perturbing the values by 25%, two sets of HbT and StO_2 are chosen for the superficial layer of brain. Similarly, for muscle the average is taken for subcutaneous fat and skin.

Superficial layer	a_{avg} (cm^{-1})	b_{avg}	Wavelength, λ (nm)	$\mu_s'(cm^{-1})$
Scalp and skull(Brain)	15.20	0.339	680, 750, 830	13.69, 13.24, 12.80
Subcutaneous fat and skin (Muscle)	32.45	0.846	680, 750, 830	25.01, 23.02, 21.12

Table 3.3: The derived parameters a and b used for the superficial layer of brain and muscle tissue and the values of μ_s' at mentioned wavelengths.

The (table 3.4) shows the HbT and StO_2 values considered to construct the layered slab models for each tissue type. In addition, in layered slab models, three thicknesses, d for the superficial layer are chosen to understand the impact of thickness in derived physiological parameters. So, for two sets of HbT and StO_2 of superficial layer and three sets of wavelength, λ and thickness, d, the total number of layered tissue models generated is 36 for each tissue type as the derived parameters of the bottom layer are not perturbed.

Tissue type	HbT(μM)	StO_2	Wavelengths, λ (nm)	Thickness,d(cm)	Number of models
Brain	S: 32.25, 53.75 B: 65	S: 0.58, 0.96 B: 0.70	680, 750, 830	S: 0.8, 1.0, 1.2 B: Semi-infinte	36
Muscle	S: 27.75, 46.25 B: 27	S: 0.53, 0.88 B: 0.70	680, 750, 830	S: 0.3, 0.6, 0.9 B: Semi-infinte	36

Table 3.4: *Calculation of the number of layered slab tissue models used for this study.[B stands for bottom and S stands for superficial layer.]*

The other parameters needed to generate the tissue models are anisotropy factor, g and the refractive index, n of the tissue media. The value of anisotropy factor is chosen 0.9 for all the tissue models (semi-infinite and layered slab) as biological tissues scatter light strongly in the forward direction [29, 30]. The refractive index of brain and muscle are 1.4 and 1.38 respectively and the refractive index of superficial layers of brain and muscle are 1.4 and 1.42 [31–33]. These tissue models will then be utilized to extract optical coefficients and derive physiological parameters from the MC simulated diffuse reflectance.

Chapter 4

Analysis and Results

Diffuse optical spectroscopy (DOS) is considered a valuable tool to facilitate noninvasive measurement of tissue oxygenation in a variety of tissues including brain and muscle. DOS technique can be used to determine relative hemodynamic changes as well as the absolute measurement of hemoglobin concentration. The relative measurements are used for functional studies to detect hemodynamic and metabolic responses to brain activation [34]. Hemoglobin concentration is an important physiological parameter as it serves is used for anemia diagnosis cancer radiotherapy and monitoring neonatal brain health [1, 2]. So, precise estimation of physiological parameters is crucial in many diagnostic and therapeutic applications. In this chapter, the physiological parameters (HbT, STO_2) will be derived from the recovered optical coefficients obtained from semi-infinite and two-layered tissue models. Then the recovered physiological parameters will be compared with the physiological parameters used in generating tissue models in chapter 3.

4.1 Derived Physiological Parameters

To derive physiological parameters, the optical coefficients are recovered for three wavelengths (680, 750 and 830nm) for each tissue models (a unique HbT and StO_2 pair). By using equation 3.1, the following linear system can be constructed (equation(4.1)). Then the solution of this linear system provides the concentration of oxyhemoglobin, C_{HbO_2} and deoxyhemoglobin, C_{Hb}. Using

the values of C_{HbO_2} and C_{Hb}, the total hemoglobin concentration, HbT and oxygen saturation, StO_2 are determined using equations 4.2 and 4.3.

$$\begin{bmatrix} \mu_a(\lambda_1) \\ \mu_a(\lambda_2) \\ \mu_a(\lambda_3) \end{bmatrix} = \begin{bmatrix} \varepsilon_{HbO_2}(\lambda_1) & \varepsilon_{Hb}(\lambda_1) \\ \varepsilon_{HbO_2}(\lambda_2) & \varepsilon_{Hb}(\lambda_2) \\ \varepsilon_{HbO_2}(\lambda_3) & \varepsilon_{Hb}(\lambda_3) \end{bmatrix} \begin{bmatrix} C_{HbO_2} \\ C_{Hb} \end{bmatrix} \tag{4.1}$$

$$HbT = C_{HbO_2} + C_{Hb} \tag{4.2}$$

$$StO_2 = \frac{C_{HbO_2}}{C_{HbO_2} + C_{Hb}} = \frac{C_{HbO_2}}{HbT} \tag{4.3}$$

4.2 Analysis: Semi-infinite Tissue Models

To determine the optical coefficients from the MC simulated diffuse reflectance spectra, the inverse model using semi-infinite diffusion theory is used that is described in chapter 2. Then the recovered optical coefficients are compared with the input optical coefficients to determine the extent of error in recovered optical coefficients. The figure 4.1 shows the average percentage of error at each source-detector separation in time domain for all the 27 models of brain and muscle. The percentage of errors in recovered optical coefficients at each source-detector separation for all the 27 semi-infinite tissue models are averaged for each tissue type. The standard deviation of percentage of errors at each source-detector separation are shown at the top of each bars. It is evident from the figure that the average percentage of errors in μ_s' decrease at long source-detector separation. The average percentage of errors in μ_a are within 1.5% considering all tissue types. Moreover, in the time domain, the percentage of error is much higher in recovered reduced scattering coefficient and that is the reason the bars for the recovered reduced scattering coefficients are scaled down by a factor 15 (figure 4.1) but the error bars are kept as its original computed values.

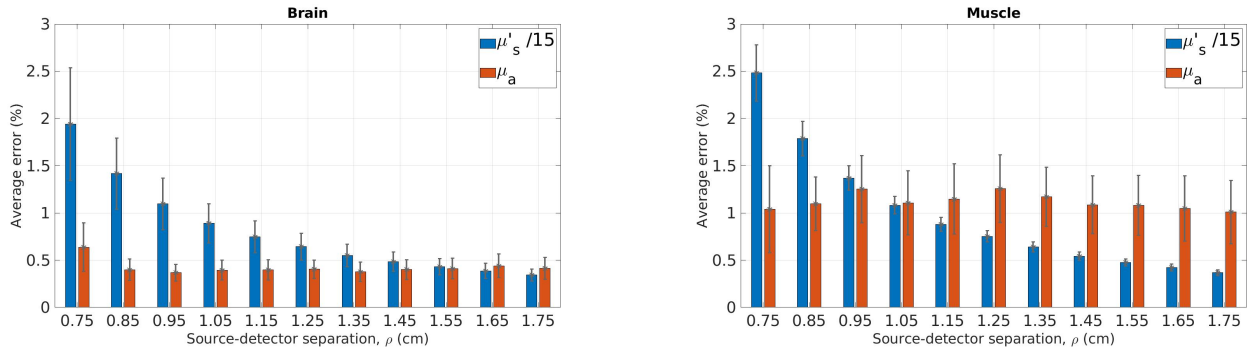

(a) *Time domain : Brain*

(b) *Time domain : Muscle*

Figure 4.1: *The figure shows the average percentage of error of the recovered absorption, μ_a and reduced scattering coefficient, μ'_s in time domain at source-detector separation from 0.75-1.75 cm. The recovered reduced scattering coefficients bars are scaled down by a factor 15 for the plotting purposes (the error bars are not scaled).*

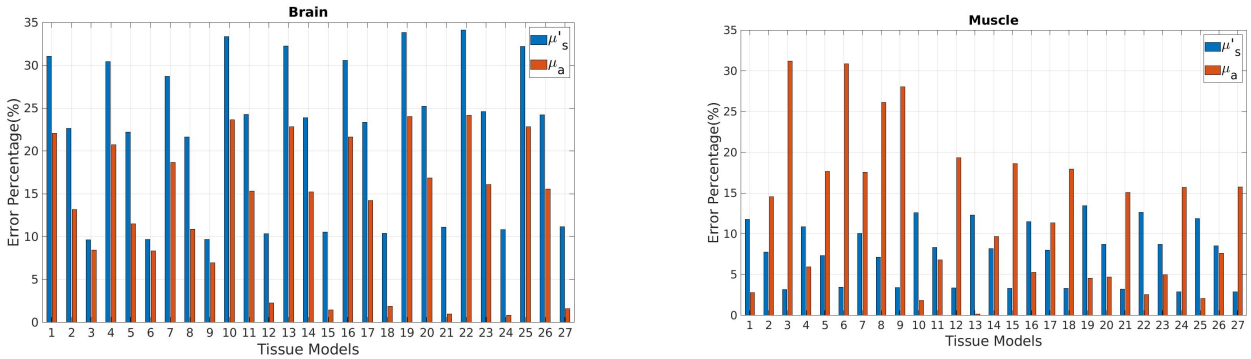

(a) *Steady state : Brain*

(b) *Steady state : Muscle*

Figure 4.2: *The figure shows percentage of error of the recovered absorption, μ_a and reduced scattering coefficient, μ'_s in steady state for all the 27 tissue models of brain and muscle.*

For the steady state measurement technique, the percentage of errors are shown in the figure 4.2 for 27 semi-infinite tissue models for brain and muscle. In the figure 4.2, each triplet represents one tissue model (unique HbT and StO_2 pair) for three different wavelengths. It is evident from the figure that the percentage of error in recovered optical coefficients is much higher for the steady state than in the time domain. It is observed that at longer wavelengths, the semi-infinite tissue models for brain shows less percentage of error in recovered optical coefficients than shorter wavelengths. In addition, For the semi-infinite models of muscle, the inverse model can estimate μ_a better at shorter wavelengths compared to longer ones. However, the inverse model can estimate μ'_s better at

longer wavelength for muscle tissue models. The probable reason behind the observation is that the muscle tissue models have lower μ_s' compared to brain tissue models, though further investigations are needed for a better understanding.

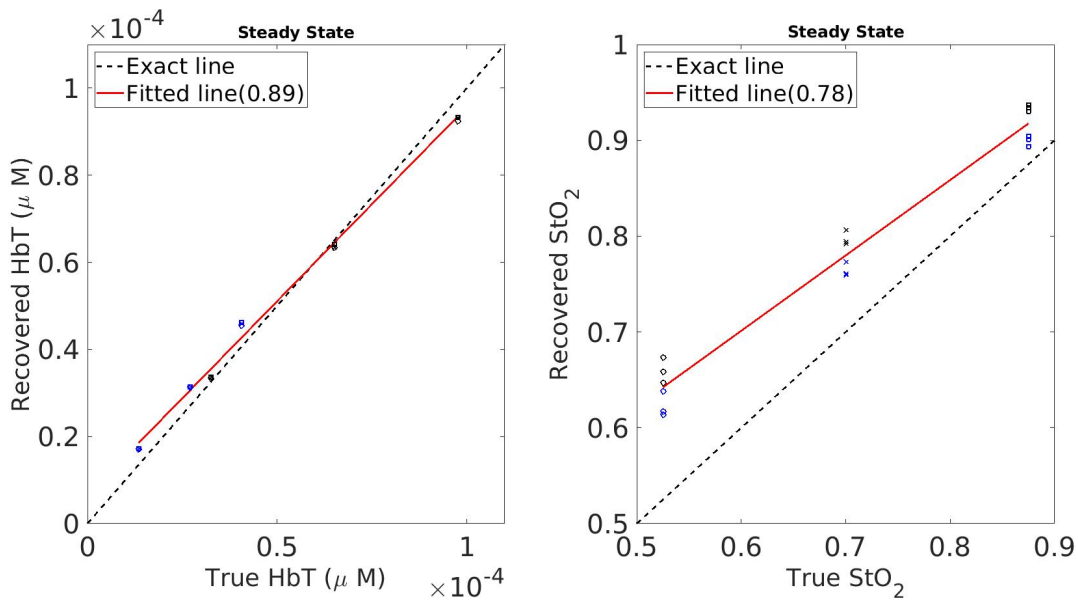

Figure 4.3: *The figure shows the recovered HbT and StO_2 in steady state. The blue points represents muscle tissue and the black points for brain tissue. The circle, cross and square points represent three different StO_2 that are considered(irrespective of color). The points are scattered into three groups as three HbT are considered for each tissue type. The red line is the fitted line and the slope of the fitted lines are mentioned in the bracket of the legend. The black line represents the exact line where true values are equal to the retrieved values from the inverse model (or, $y = x$; slope = 1). In the legend, the slope of fitted line is shown inside the bracket.*

The figure 4.3 shows the recovered hemoglobin concentration and oxygen saturation for steady state measurement and the figure 4.4 are for the time domain measurement. For the time domain analysis, three source-detector separations (0.75, 1.25 and 1.75 cm) have been used. The figure 4.3 depicts in time domain, the inverse model using diffusion theory can predict HbT and StO_2 pretty accurately for the semi-infinite tissue models as the slope of fitted line and exact line are close. However, for the steady state measurements, there is a deviation from the exact line (figure 4.3) which signifies that the time-domain measurement can estimate HbT and StO_2 better.

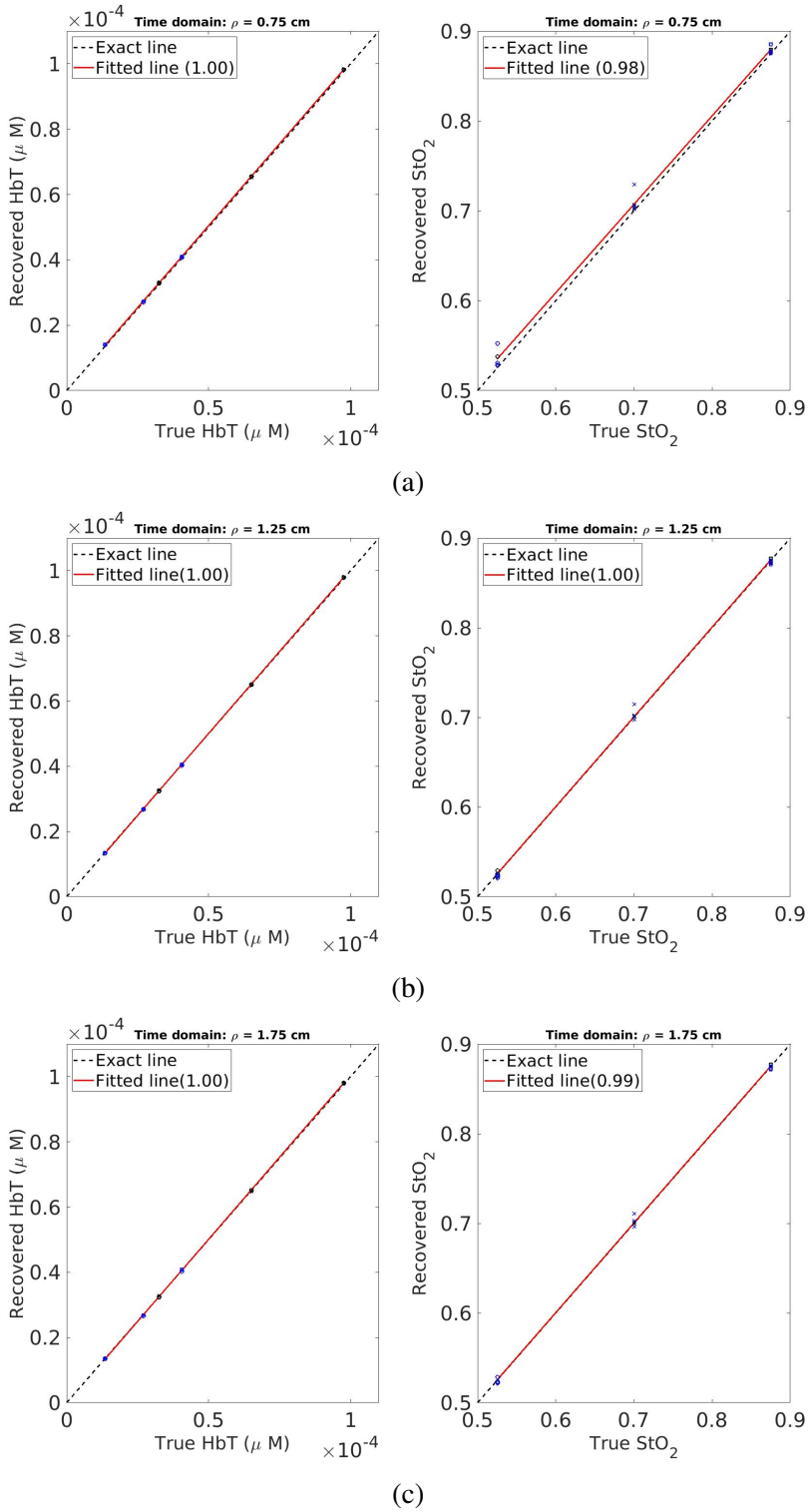

Figure 4.4: *The figure shows the recovered HbT and StO_2 in time domain. The points and lines properties are kept the same as in the figure 4.3. Each row represents the data at each source-detector separation (ρ = 0.75, 1.25 and 1.75 cm). The first column of figures are for recovered HbT and second column of figures are for recovered StO_2.*

4.3 Analysis: Layered Slab Tissue Models

For the two-layered slab models, the goal is to recover the optical coefficients of the bottom layer (brain and muscle) to derive the physiological parameters. So, the inverse model based on semi-infinite diffusion theory is used to extract optical coefficients from the MC simulated reflectance of two layered slab models. However, to check the goodness of the fit of the diffuse reflectance spectra from the layered slab models, the residuals are calculated to show how they vary with time. The residual is defined as the difference between the MC simulated reflectance and the estimated data

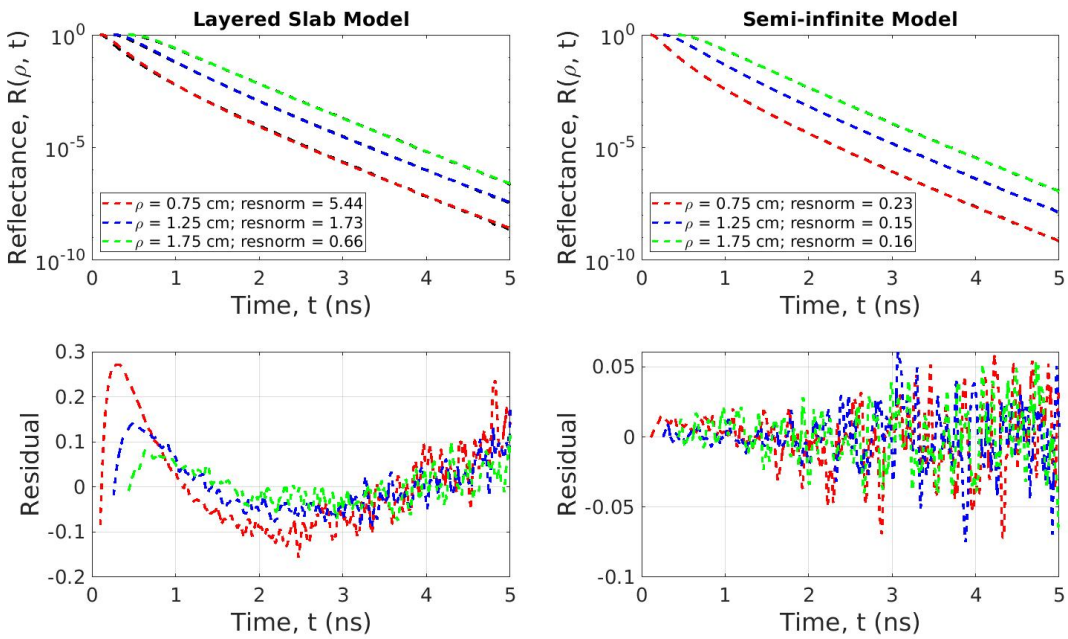

Figure 4.5: *In the figure, the first column is for layered slab model and the second column for the semi-infinite model. The first row shows the fitted data with the MC simulated diffuse reflectance in time domain from a layered slab and a semi-infinite model. The optical coefficients for the layered slab model are: S: $\mu_a = 0.08\ cm^{-1}$, $\mu_s' = 13.69\ cm^{-1}$; B: $\mu_a = 0.13\ cm^{-1}$, $\mu_s' = 15.78\ cm^{-1}$. [S - superficial layer, B - bottom layer.] The semi-infinite model has the same optical properties as the bottom layer of the layered slab model. In the legend of the first row, the squared norm of the residuals are mentioned. The second row shows the change of the residuals with time.*

from the inverse model. In the figure 4.5, a layered slab model is compared with a semi-infinite model that has the same optical properties as the bottom layer of the layered slab model. It is

observed that the "resnorm", that is the squared norm of the residuals tend to decrease as the source-detector separation increases for both layered and semi-infinite tissue model. However, the residuals for the layered slab model increase sharply upto a maximum value and then start to decrease whereas the semi-infinite models fluctuate more rapidly at early time. This points out that the superficial layer has an observable impact on the diffuse reflectance spectra.

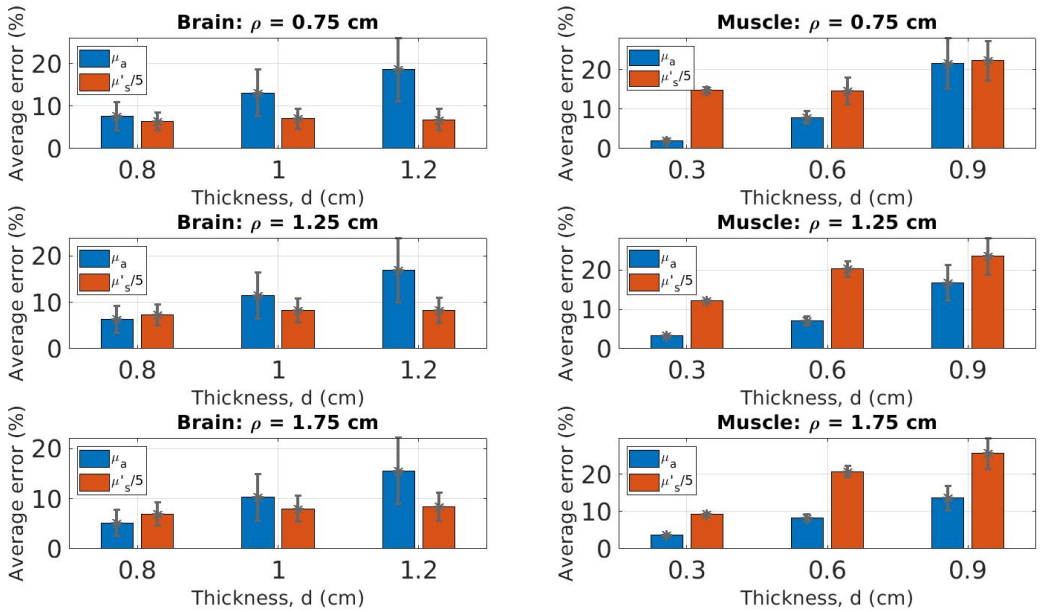

Figure 4.6: *The average percentage of error of recovered optical coefficients with respect to the thickness of the superficial layer at* $\rho = 0.75$, 1.25 *and* 1.75 *cm in time domain.*

The optical coefficients extracted from the steady state measurements for the semi-infinite models have a relatively high percentage of error than the time domain measurements. So, for the layered slab models, the analysis is based solely on the time domain measurements. So, the inverse model using semi-infinite diffusion theory is utilized to estimate the optical coefficients of the bottom layer (brain or muscle). The figure 4.6 shows the average percentage of error in recovered optical coefficients from the layered slab models at source-detector separation, ρ = 0.75, 1.25 and 1.75 cm for each thicknesses of the superficial layer of brain and muscle. For layered slab models, 12 models are generated for a specific thickness. The average error is calculated by taking the

percentage of error in recovered optical coefficients from time domain measurements for 12 tissue models at each thicknesses. It is evident from the figure that the average percentage of error increases with the thickness of the superficial layer. In addition, the inverse model produces high percentage of errors in estimating reduced scattering coefficients, μ_s' than absorption coefficients, μ_a. Considering all the thicknesses and source-detector separations, the average percentage of error of μ_a varies within 5.18 to 18.64% whereas μ_s' varies within 1.9 to 93.1% for layered slab brain tissue models. However, for muscle tissue models the average percentage of error of μ_a varies within 2.06 to 21.59% whereas the μ_s' varies within 45.93 to 127.7%. The difference of μ_s' between the superficial and bottom layer is much higher for muscle tissues than brain tissues while simulating diffuse reflectance and that could the reason for the huge percentage of error in recovered μ_s'.

From the total 36 layered slab tissue models of each tissue type(brain and muscle), 12 unique tissue models are generated at each thickness (table 3.4). In other words, 12 sets of optical coefficients are recovered for 3 different wavelengths at a certain thickness. Then by taking the percentage of error of all 4 sets, the average error is determined. The error bars are calculated using the the standard deviation of percentage of errors of each individual models. The figure 4.7 shows how the average percentage of error in recovered physiological parameters change with the thickness of the superficial layer for brain and muscle tissue models individually. However, at source-detector separation, ρ = 0.75 and 1.25cm, the average error of the retrieved hemoglobin concentration is higher for muscle tissue with the thickness of 0.9 cm compared to the retrieved values from brain layered slab models at 1.2 cm. This signifies the fact that the thickness of the superficial layer is not the only factor that contributes to the error. The relative difference of optical coefficients between the layers may have an impact in recovering physiological parameters. Moreover, the inverse model using semi-infinite diffusion theory can estimate the absorption coefficients much better than the reduced scattering coefficients of the bottom layer of the layered slab models (figure 4.6). So, the percentage of error in recovered total hemoglobin concentration and oxygen saturation varies within 1.6 to 19.6% and the 0.29 to 11.9% considering all the thicknesses and source-detector separations.

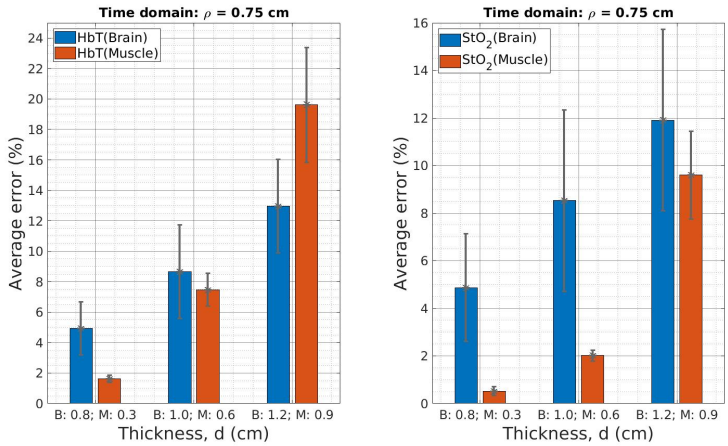

(a)

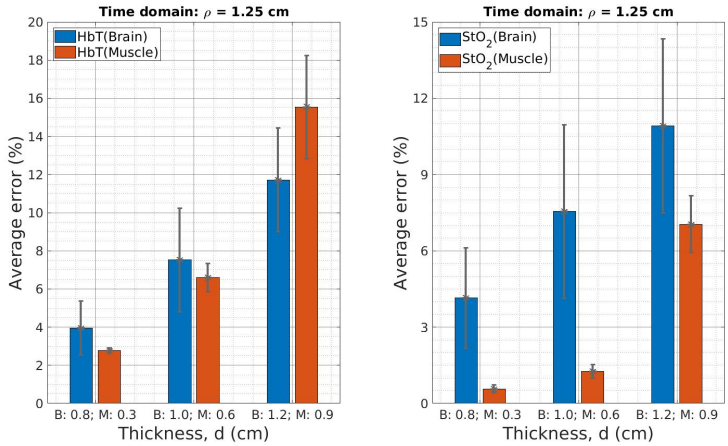

(b)

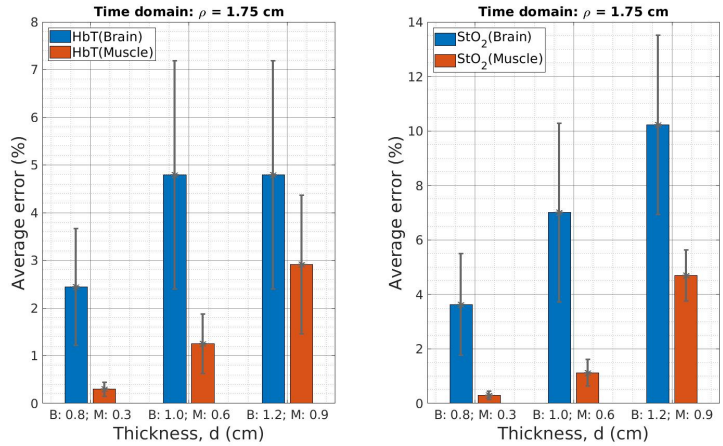

(c)

Figure 4.7: *The average percentage of error in recovered HbT and StO_2 for different thicknesses of the superficial layer at $\rho = 0.75$ (row 1), 1.25 (row 2) and 1.75cm (row 3). The first column are for HbT and the second column is for StO_2. The factors shown in the legend are used to make the bar visible.*

Chapter 5

Conclusion

In this study, the aim was to assess the accuracy of semi-infinite diffusion theory in measuring optical coefficients and physiological parameters for layered slab models of brain and muscle. Layer based MC model was used to simulate photon propagation inside a two-layered slab tissue models. Simulations results were then analyzed using semi-infinite homogeneous model, which is one of the most widespread analytical model to analyze diffuse reflectance spectra because of its low level of complexity. The recovered reduced scattering coefficient extracted by semi-infinite diffusion theory showed more percentage of error than the retrieved absorption coefficient. The retrieved optical coefficients were affected by the presence of superficial layers and the thickness of the superficial layer. The variations of absorption coefficients due to the superficial layer were reflected in retrieved hemodynamic parameters.The presented results highlight the need for more complex methods of analysis which may allow to reduce the influence of superficial layers in retrieved physiological parameters, for example, in future the diffusion equation for the layered slab models can be utilized [35, 36].

5.1 Summary of the Findings

The findings of this study can be summarized as below:

1. The analysis of semi-infinite tissue models using semi-infinite diffusion theory shows less

margin of error compared to the steady state measurements.

2. From the analysis of two-layered slab models, it is observed that the percentage of error increases with the thickness of the superficial layer.

3. However, it is also observed that the thickness of the superficial layer is not the only factor that contributes to the error. The relative difference of optical coefficients between the layers may have an impact in recovering physiological parameters.

5.2 Future Directions

In this study, derived parameters using the retrieved absorption coefficients are studied. However, there are other two parameters "a"and "b"that can be computed from the recovered reduced scattering coefficients. So, the equation 3.3 can be rewritten as follows:

$$\log(\mu_s'(\lambda)) = \log(a) - b\log(\frac{\lambda}{500(nm)}) \tag{5.1}$$

The reduced scattering coefficient is recovered from three different wavelengths. Therefore, the following linear system can be constructed using the retrieved reduced scattering coefficients:

$$\begin{bmatrix} 1 & -\log(\frac{\lambda_1}{500}) \\ 1 & -\log(\frac{\lambda_2}{500}) \\ 1 & -\log(\frac{\lambda_3}{500}) \end{bmatrix} \begin{bmatrix} \log(a) & \log(a) & \log(a) \\ b & b & b \end{bmatrix} = \begin{bmatrix} \log[\mu_s'(\lambda_1)] \\ \log[\mu_s'(\lambda_2)] \\ \log[\mu_s'(\lambda_3)] \end{bmatrix} \tag{5.2}$$

By solving the equation 5.2, the derived parameters "a"and "b"can be recovered. As derived parameters "a"and "b"can give us information about the structure of the biological tissue, the comparison between the input and retrieved derived parameters from the reduced scattering coefficient may help to understand the structural differences between the input and recovered tissue model. In addition,

the anisotropy factor, g can be calculated from the recovered "a"and "b"at each wavelength using the following equation:

$$\log(\mu_s'(\lambda)) = 1 - \frac{a}{\mu_s}.(\frac{\lambda}{500})^{-b} \tag{5.3}$$

The anisotropy factor was chosen 0.9 as the biological tissues are highly forward scattering [29, 30]. In the literature, it is reported that the anisotropy factor, g depends on the wavelength and absorption [37–41]. Therefore, it would be an interesting avenue to explore how anisotropy factor changes with wavelength and hemoglobin concentration.

To extract optical coefficients from the time domain measurements, the diffuse reflectance spectra were fitted from the time of maximum reflectance to the time of minimum reflectance measured. However, for reflectance type measurements, early photons travel a short distance within the medium and thus, these photons probe mostly the superficial layer of a tissue. The late photons probe into the deeper layer of tissue. So, different time intervals of the diffuse reflectance spectra can give information about the optical properties at different thicknesses within the tissue medium. In future, the diffuse reflectance spectra can be analyzed by dividing the diffuse reflectance spectra into several time intervals starting from the time of maximum reflectance. Utilizing the semi-infinite theory based inverse model, the optical coefficients from each interval can be recovered. Then the correlation among the retrieved parameters from each time intervals can be studied to understand the tissue hemodynamics at different depths of the tissue medium. This time-gated approach is developed and studied for various applications in biomedical optics, such as, blood oxygenation in the arm during a motor activity [42], cerebral hemodynamics during brain activation [43], neonatal and adult brain imaging [44–46]. So, it would be worth exploring to study the depth sensitivity of time domain diffuse reflectance measurements.

In this study, the layered slab models are analyzed by perturbing the hemoglobin concentration, HbT and oxygen saturation, StO_2 of the superficial layer. Then using the inverse model, the optical

coefficients of the bottom layer, that are brain and muscle, are recovered. Then from the recovered optical coefficients, the physiological parameters are derived. So, this study aids to understand how the hemodynamic changes in the superficial layer may have an impact on the recovered parameters of brain and muscle. By analyzing the two-layered slab models, it is observed that the relative differences of the optical coefficients between the superficial and bottom layer have an impact on estimating the physiological parameters. To understand how the relative differences in optical coefficients have an impact, a two-layered slab models can be constructed where the bottom layer and the superficial layer have the same physiological parameters (same as semi-infinite model as the layers have the same optical properties). The physiological parameters of the superficial layer then can be perturbed by $10 - 15\%$ on both side of this base value (that is same as the bottom layer at first) for the superficial layer. In this method, it can be observed that how the relative differences of the optical coefficients are making an impact on the recovered physiological parameters. It is straightforward to understand that the error percentage of the physiological parameters will be minimum as the relative difference of the optical coefficients is zero and semi-infinite diffusion theory is used for the analysis. However, it can be observed how the percentage of error in recovered physiological parameters vary with the relative differences, for example, in absorption coefficients. In addition, Amendola et. al studied the recovered physiological parameters in three hemodynamic scenarios (ischemia, hyperoxygenation and hypoventilation) [47]. Therefore, it would be quite fascinating to study the hemodynamic parameters in terms of the relative differences in optical coefficients between the tissue layers.

Bibliography

[1] C. D. Karakochuk, S. Y. Hess, D. Moorthy, S. Namaste, M. E. Parker, A. I. Rappaport, R. Wegmüller, O. Dary, and H. M. H. W. Group, "Measurement and interpretation of hemoglobin concentration in clinical and field settings: a narrative review," *Annals of the New York Academy of Sciences*, vol. 1450, no. 1, pp. 126–146, 2019.

[2] C. M. Hoff, "Importance of hemoglobin concentration and its modification for the outcome of head and neck cancer patients treated with radiotherapy," *Acta Oncologica*, vol. 51, no. 4, pp. 419–432, 2012.

[3] S. Koike, Y. Nishimura, R. Takizawa, N. Yahata, and K. Kasai, "Near-infrared spectroscopy in schizophrenia: a possible biomarker for predicting clinical outcome and treatment response," *Frontiers in Psychiatry*, vol. 4, p. 145, 2013.

[4] B. Sukrat, C. Wilasrusmee, B. Siribumrungwong, M. McEvoy, C. Okascharoen, J. Attia, and A. Thakkinstian, "Hemoglobin concentration and pregnancy outcomes: a systematic review and meta-analysis," *BioMed Research International*, vol. 2013, 2013.

[5] T. Parker-Pope, "What's a pulse oximeter, and do i really need one at home?." `https://www.nytimes.com/2020/04/24/well/live/coronavirus-pulse-oximeter-oxygen.html`, 2020.

[6] M. Ferrari and V. Quaresima, "A brief review on the history of human functional near-infrared spectroscopy (fnirs) development and fields of application," *Neuroimage*, vol. 63, no. 2, pp. 921–935, 2012.

[7] A. P. Gibson, J. C. Hebden, and S. R. Arridge, "Recent advances in diffuse optical imaging," *Physics in Medicine & Biology*, vol. 50, no. 4, p. R1, 2005.

[8] A. Pellicer and M. del Carmen Bravo, "Near-infrared spectroscopy: a methodology-focused review," in *Seminars in fetal and neonatal medicine*, vol. 16, pp. 42–49, Elsevier, 2011.

[9] R. H. Wilson, K. Vishwanath, and M.-A. Mycek, "Optical methods for quantitative and label-free sensing in living human tissues: principles, techniques, and applications," *Advances in Physics: X*, vol. 1, no. 4, pp. 523–543, 2016.

[10] A. J. Welch, M. J. Van Gemert, *et al.*, *Optical-thermal response of laser-irradiated tissue*, vol. 2. Springer, 2011.

[11] F. Martelli, S. Del Bianco, A. Ismaelli, and G. Zaccanti, *Light propagation through biological tissue and other diffusive media: theory, solutions and software*, vol. 10. SPIE press Bellingham, 2010.

[12] S. L. Jacques and B. W. Pogue, "Tutorial on diffuse light transport," *Journal of Biomedical Optics*, vol. 13, no. 4, p. 041302, 2008.

[13] A. Villringer, J. Planck, C. Hock, L. Schleinkofer, and U. Dirnagl, "Near infrared spectroscopy (nirs): a new tool to study hemodynamic changes during activation of brain function in human adults," *Neuroscience Letters*, vol. 154, no. 1-2, pp. 101–104, 1993.

[14] A. Liemert and A. Kienle, "Exact and efficient solution of the radiative transport equation for the semi-infinite medium," *Scientific Reports*, vol. 3, no. 1, pp. 1–7, 2013.

[15] A. Ishimaru, *Wave propagation and scattering in random media*, vol. 2. Academic press New York, 1978.

[16] T. J. Farrell, M. S. Patterson, and B. Wilson, "A diffusion theory model of spatially resolved, steady-state diffuse reflectance for the noninvasive determination of tissue optical properties in vivo," *Medical Physics*, vol. 19, no. 4, pp. 879–888, 1992.

[17] A. Kienle and M. S. Patterson, "Improved solutions of the steady-state and the time-resolved diffusion equations for reflectance from a semi-infinite turbid medium," *Journal of the Optical Society America A*, vol. 14, no. 1, pp. 246–254, 1997.

[18] C. Zhu and Q. Liu, "Review of monte carlo modeling of light transport in tissues," *Journal of Biomedical Optics*, vol. 18, no. 5, p. 050902, 2013.

[19] S. E. Skipetrov and S. S. Chesnokov, "Analysis, by the monte carlo method, of the validity of the diffusion approximation in a study of dynamic multiple scattering of light in randomly inhomogeneous media," *Quantum Electronics*, vol. 28, no. 8, p. 733, 1998.

[20] R. J. Hennessy, S. L. Lim, M. K. Markey, and J. W. Tunnell, "Monte carlo lookup table-based inverse model for extracting optical properties from tissue-simulating phantoms using diffuse reflectance spectroscopy," *Journal of Biomedical Optics*, vol. 18, no. 3, p. 037003, 2013.

[21] J. L. Sandell and T. C. Zhu, "A review of in-vivo optical properties of human tissues and its impact on pdt," *Journal of Biophotonics*, vol. 4, no. 11-12, pp. 773–787, 2011.

[22] K. Vishwanath, *Computational modeling of time-resolved fluorescence transport in turbid media for non-invasive clinical diagnostics*. PhD thesis, 2005.

[23] Q. Fang, "Mesh-based monte carlo method using fast ray-tracing in plücker coordinates," *Biomedical Optics Express*, vol. 1, no. 1, pp. 165–175, 2010.

[24] D. A. Boas, J. P. Culver, J. J. Stott, and A. K. Dunn, "Three dimensional monte carlo code for photon migration through complex heterogeneous media including the adult human head," *Optics Express*, vol. 10, no. 3, pp. 159–170, 2002.

[25] K. Vishwanath and M.-A. Mycek, "Time-resolved photon migration in bi-layered tissue models," *Optics Express*, vol. 13, no. 19, pp. 7466–7482, 2005.

[26] S. L. Jacques, "Optical properties of biological tissues: a review," *Physics in Medicine & Biology*, vol. 58, no. 11, p. R37, 2013.

[27] S. Prahl, "Optical Absorption of Hemoglobin." https://omlc.org/spectra/hemoglobin/, 1999.

[28] L. Gagnon, C. Gauthier, R. D. Hoge, F. Lesage, J. J. Selb, and D. A. Boas, "Double-layer estimation of intra-and extracerebral hemoglobin concentration with a time-resolved system," *Journal of Biomedical Optics*, vol. 13, no. 5, p. 054019, 2008.

[29] W.-F. Cheong, S. A. Prahl, and A. J. Welch, "A review of the optical properties of biological tissues," *IEEE Journal of Quantum Electronics*, vol. 26, no. 12, pp. 2166–2185, 1990.

[30] A. D. Kim and J. B. Keller, "Light propagation in biological tissue," *Journal of the Optical Society America A*, vol. 20, no. 1, pp. 92–98, 2003.

[31] J. J. Dirckx, L. C. Kuypers, and W. F. Decraemer, "Refractive index of tissue measured with confocal microscopy," *Journal of Biomedical Optics*, vol. 10, no. 4, p. 044014, 2005.

[32] A. N. Bashkatov, E. A. Genina, and V. V. Tuchin, "Optical properties of skin, subcutaneous, and muscle tissues: a review," *Journal of Innovative Optical Health Sciences*, vol. 4, no. 01, pp. 9–38, 2011.

[33] P. Sawosz, S. Wojtkiewicz, M. Kacprzak, W. Weigl, A. Borowska-Solonynko, P. Krajewski, K. Bejm, D. Milej, B. Ciszek, R. Maniewski, *et al.*, "Human skull translucency: post mortem studies," *Biomedical Optics Express*, vol. 7, no. 12, pp. 5010–5020, 2016.

[34] B. Hallacoglu, A. Sassaroli, S. Fantini, M. Wysocki, E. Guerrero-Berroa, M. S. Beeri, V. Haroutunian, M. Shaul, I. H. Rosenberg, and A. Troen, "Absolute measurement of cerebral optical coefficients, hemoglobin concentration and oxygen saturation in old and young adults with near-infrared spectroscopy," *Journal of Biomedical Optics*, vol. 17, no. 8, p. 081406, 2012.

[35] A. Kienle, M. S. Patterson, N. Dögnitz, R. Bays, G. Wagnieres, and H. van Den Bergh, "Noninvasive determination of the optical properties of two-layered turbid media," *Applied Optics*, vol. 37, no. 4, pp. 779–791, 1998.

[36] F. Martelli, A. Sassaroli, Y. Yamada, and G. Zaccanti, "Analytical approximate solutions of the time-domain diffusion equation in layered slabs," *Journal of the Optical Society America A*, vol. 19, no. 1, pp. 71–80, 2002.

[37] M. Friebel, A. Roggan, G. J. Müller, and M. C. Meinke, "Determination of optical properties of human blood in the spectral range 250 to 1100 nm using monte carlo simulations with hematocrit-dependent effective scattering phase functions," *Journal of Biomedical Optics*, vol. 11, no. 3, p. 034021, 2006.

[38] D. Fukutomi, K. Ishii, and K. Awazu, "Determination of the scattering coefficient of biological tissue considering the wavelength and absorption dependence of the anisotropy factor," *Optical Review*, vol. 23, no. 2, pp. 291–298, 2016.

[39] G. Hall, S. L. Jacques, K. W. Eliceiri, and P. J. Campagnola, "Goniometric measurements of thick tissue using monte carlo simulations to obtain the single scattering anisotropy coefficient," *Biomedical Optics Express*, vol. 3, no. 11, pp. 2707–2719, 2012.

[40] A. Fernandez-Oliveras, M. Rubiño, and M. Perez, "Scattering anisotropy measurements in dental tissues and biomaterials," *Journal of the European Optical Society-Rapid publications*, vol. 7, 2012.

[41] E. Zamora-Rojas, B. Aernouts, A. Garrido-Varo, D. Pérez-Marín, J. E. Guerrero-Ginel, and W. Saeys, "Double integrating sphere measurements for estimating optical properties of pig subcutaneous adipose tissue," *Innovative Food Science & Emerging Technologies*, vol. 19, pp. 218–226, 2013.

[42] E. M. Hillman, J. C. Hebden, M. Schweiger, H. Dehghani, F. E. Schmidt, D. T. Delpy, and S. R. Arridge, "Time resolved optical tomography of the human forearm," *Physics in Medicine & Biology*, vol. 46, no. 4, p. 1117, 2001.

[43] J. J. Selb, J. J. Stott, M. A. Franceschini, A. G. Sorensen, and D. A. Boas, "Improved sensitivity to cerebral hemodynamics during brain activation with a time-gated optical system: analytical

model and experimental validation," *Journal of Biomedical Optics*, vol. 10, no. 1, p. 011013, 2005.

[44] J. C. Hebden, A. Gibson, R. M. Yusof, N. Everdell, E. M. Hillman, D. T. Delpy, S. R. Arridge, T. Austin, J. H. Meek, and J. S. Wyatt, "Three-dimensional optical tomography of the premature infant brain," *Physics in Medicine & Biology*, vol. 47, no. 23, p. 4155, 2002.

[45] J. Steinbrink, H. Wabnitz, H. Obrig, A. Villringer, and H. Rinneberg, "Determining changes in nir absorption using a layered model of the human head," *Physics in Medicine & Biology*, vol. 46, no. 3, p. 879, 2001.

[46] A. Liebert, H. Wabnitz, J. Steinbrink, H. Obrig, M. Moeller, R. Macdonald, and H. Rinneberg, "Intra-and extracerebral changes of hemoglobin concentrations by analysis of moments of distributions of times of flight of photons," in *European Conference on Biomedical Optics*, p. 5138_126, Optical Society of America, 2003.

[47] C. Amendola, L. Spinelli, D. Contini, A. De Carli, C. Martinelli, M. Fumagalli, and A. Torricelli, "Accuracy of homogeneous models for photon diffusion in estimating neonatal cerebral hemodynamics by td-nirs," *Biomedical Optics Express*, vol. 12, no. 4, pp. 1905–1921, 2021.